

26

Abstract

27 Objective assessment of the sensory pathways is crucial for understanding their development
28 across the lifespan and how they may be affected by neurodevelopmental disorders (e.g.,
29 autism) and neurological pathologies (e.g., stroke, multiple sclerosis, etc.). Quick and passive
30 measurements, for example using electroencephalography (EEG), are especially important
31 when working with infants and young children, and with patient populations having
32 communication deficits (e.g., aphasia). However, many EEG paradigms are limited to
33 measuring activity from one sensory domain at a time, may be time consuming, and target only
34 a subset of possible responses from that particular sensory domain (e.g., only auditory
35 brainstem responses or only auditory P1-N1-P2 evoked potentials). Thus, we developed a new
36 multisensory paradigm that enables simultaneous, robust, and rapid (6-12 minute)
37 measurements of both auditory and visual EEG activity, including auditory brainstem responses
38 (ABRs), auditory and visual evoked potentials, as well as auditory and visual steady-state
39 responses. This novel method allows us to examine neural activity at various stations along the
40 auditory and visual hierarchies with an ecologically valid continuous speech stimulus, while an
41 unrelated video is playing. Both the speech stimulus and the video can be customized for any
42 population of interest. Furthermore, by using two simultaneous visual steady-state stimulation
43 rates, we demonstrate the ability of this paradigm to track both parafoveal and peripheral visual
44 processing concurrently. We report results from twenty-five healthy young adults, which
45 validate this new paradigm.

46

47 **Keywords:** auditory, visual, evoked potentials, steady-state responses, Cheech

48

49

50 **New and Noteworthy**

51 A novel electroencephalography (EEG) paradigm enables the rapid, reliable, and non-invasive
52 assessment of neural activity along both auditory and visual pathways concurrently. The
53 paradigm uses an ecologically valid continuous speech stimulus for auditory evaluation and can
54 simultaneously track visual activity to both parafoveal and peripheral visual space. This new
55 methodology may be particularly appealing to researchers and clinicians working with infants
56 and young children, and with patient populations with limited communication abilities.

57

58

59

60

61

62

63

64

65

66

67

68

69

70

Introduction

71 To understand sensory development across the lifespan and the impact of
72 neurodevelopmental disorders (e.g., autism spectrum) or neurological pathologies and insults
73 (e.g., multiple sclerosis, stroke, etc.) on sensory systems, the ability to objectively measure the
74 functioning of sensory pathways is critical. Reliable objective and passive measures are
75 especially important when working with individuals with limited communication abilities (e.g.,
76 infants, individuals with aphasia, etc.). Furthermore, from a research and potentially a clinical
77 standpoint, the ability to objectively, non-invasively, and quickly assess the functioning of visual
78 and auditory pathways can provide important information about an individual that is not readily
79 available through behavioral testing. For instance, this information may be used to link
80 individual differences in a child's sensory development with his or her cognitive development, or
81 to guide research and development of individualized clinical interventions. In our case, we
82 developed the paradigm described herein to examine sensory development in normal-hearing
83 children and children with cochlear implants. In the current manuscript, we present data from
84 healthy young adults as validation of the methodology.

85 The objective of the current paradigm was to record numerous clinically important
86 auditory and visual neural responses simultaneously and quickly, while the participant watched
87 an unrelated video. While several non-invasive neuroimaging techniques could be used to
88 achieve this goal, we chose electroencephalography (EEG) for its many practical advantages.
89 EEG has excellent (sub-millisecond) temporal resolution, which is essential to examine neural
90 activity along the auditory hierarchy from the brainstem to the cortex and to track auditory and
91 visual steady-state responses. Furthermore, EEG is safe and has been used for decades in
92 clinical settings. It is portable and relatively inexpensive to use, unlike
93 magnetoencephalography (MEG) and functional magnetic resonance imaging (fMRI). In
94 addition, EEG poses no contra-indications unlike fMRI, with which many metallic medical

95 devices or implants may be incompatible due to safety risks. Finally, EEG can measure activity
96 from deep brain structures, particularly the auditory brainstem, unlike functional near-infrared
97 spectroscopy (fNIRS) which is limited to superficial cortical regions. Thus, for the purposes of
98 our objective, the above-mentioned strengths of EEG outweighed its primary weakness, that is,
99 poor spatial resolution.

100 Many EEG protocols are limited to collecting a subset of neural responses in one
101 sensory modality at a time. Furthermore, especially in the auditory modality, there has been
102 increased interest in assessing relationships between the early brainstem EEG activity to the
103 later cortical responses, and eventually to speech perception, within individuals. Paradigms that
104 have been designed for this purpose are either time consuming (due to the longer inter-stimulus
105 interval needed for the later responses juxtaposed with the large number of sweeps required for
106 reliable early brainstem responses, if recording both types of responses simultaneously) or are
107 unable to record the early and later responses simultaneously (e.g., Bidelman 2015; Bidelman
108 et al. 2013; Krishnan et al. 2012; Musacchia et al. 2008; Woods et al. 1993). A paradigm
109 recently developed by Slugocki et al. (2017) simultaneously measured both subcortical and
110 cortical responses (including P3a and mismatch negativity (MMN)) to auditory stimuli; however,
111 the recording time was relatively long (approx. 40 minutes) and the stimuli were created using
112 amplitude-modulated tones. Another group developed an EEG paradigm to simultaneously
113 record potentials including the auditory N1, MMN, P300, and N400 in about 5 minutes, using
114 both tone and speech stimuli (Sculthorpe-Petley et al. 2015); however, this paradigm was
115 limited to cortical potentials in response to auditory stimuli only. In contrast, the EEG paradigm
116 described herein, allows for the rapid recording of both auditory and visual responses
117 simultaneously, using a specially engineered continuous speech stimulus and an interspersed
118 visual stimulus. The continuous speech stimulus allows for the examination of auditory EEG
119 activity from brainstem to cortex and under more naturalistic conditions, compared to other

120 frequently used stimuli like clicks, tones, and consonant-vowel syllables. The visual stimulus
121 permits assessment of transient evoked and steady-state visual responses.

122 It is important to mention that this paradigm significantly builds upon previous work
123 conducted by our group (Miller et al. 2017). Previously, a continuous speech stimulus was used
124 and demonstrated the feasibility of simultaneously obtaining auditory evoked responses along
125 the auditory pathway, from the brainstem to the cortex. This set the foundation for the current
126 methodology. Novel aspects of the EEG paradigm presented in this report include the following:
127 First, in conjunction with the continuous speech stimulus, unrelated visual flicker stimuli were
128 used to obtain both auditory and visual EEG responses simultaneously. Second, in the current
129 implementation, the use of a silent video, which engages attention and is unrelated to the
130 auditory and visual stimuli, makes the paradigm suitable to different populations (e.g., young
131 children). This is a critical validation step, to determine which responses can be reliably
132 observed – even when the auditory and visual stimuli are not necessarily attended.

133 To introduce the current methodology, we provide an overview of the auditory and visual
134 responses that the EEG paradigm was designed to measure, including the time course for each
135 response, how the response can be elicited, and the putative neural generators for each
136 response. The following sections therefore illustrate the scope of our approach and motivate
137 many technical details of the design and analysis, described next. It also serves as a brief
138 tutorial for readers unfamiliar with auditory and visual EEG. (For a thorough discussion of these
139 topics, see Halgren 1990; Hall 2007; Luck 2014.)

140 **Auditory Responses**

141 The stimulus used in the current EEG paradigm was designed to enable the
142 simultaneous recording of the auditory brainstem response (ABR), the middle latency response

143 (MLR), the long latency response (LLR), as well as the auditory steady-state response (ASSR),
144 all in the context of naturalistic, intelligible, and continuous spoken language.

145 The stereotyped ABR consists of seven positive peaks (Waves I to VII) that occur within
146 10 ms following the onset of a brief sound; Wave V generally has the largest amplitude of these
147 peaks (Jewett and Williston 1971). Often, the ABR is elicited with a click stimulus (e.g., Jewett
148 and Williston 1971; Pratt and Sohmer 1976), but tone pips (e.g., Suzuki et al. 1977; Weber and
149 Folsom 1977; Woldorff and Hillyard 1991), chirps (e.g., Bell et al. 2002a; Dau et al. 2000;
150 Elberling and Don 2008), and brief speech sounds (e.g., consonant-vowel syllables, Krizman et
151 al. 2010) can elicit ABRs as well. The ABR reflects the neural response to sound ascending the
152 auditory pathway (for a review, see Moore 1987), from the eighth cranial nerve (Wave I)
153 (Hashimoto et al. 1979; Moller et al. 1982; Moller et al. 1981; Starr and Hamilton 1976) to the
154 lateral lemniscus and inferior colliculus (Waves IV and V) (Moore 1987; Starr and Hamilton
155 1976).

156 The MLR is the next set of waveforms as the acoustic representation ascends along the
157 auditory pathway. The MLR comprises two negative peaks interleaved with two positive peaks
158 (Na, Pa, Nb, and Pb), which occur from approximately 15 to 60 ms after sound onset (Geisler et
159 al. 1958; Goldstein and Rodman 1967). Some studies have also reported waves N_0 and P_0 ,
160 which occur earlier, around 8-9 and 12-14 ms, respectively (Mendel and Goldstein 1969; Picton
161 et al. 1974; Yoshiura et al. 1996). Clicks, tones, and chirps can elicit the MLR (e.g., Bell et al.
162 2002b; Mendel and Goldstein 1969; Picton et al. 1974). Taken together, source modeling
163 (Pelizzone et al. 1987; Rupp et al. 2002; Scherg and Von Cramon 1986; Yoshiura et al. 1996;
164 1995), intracranial (Celesia 1976; Lee et al. 1984; Liegeois-Chauvel et al. 1994), and lesion
165 (Kileny et al. 1987; Kraus et al. 1982) studies have shown that the MLR is primarily generated in
166 supratemporal cortex. Additionally, sub-cortical activity likely contributes to at least the earlier
167 MLR components, especially the Na (Hashimoto 1982; Kileny et al. 1987).

168 The LLR is the final set of auditory evoked potentials observed in the cascade. A
169 stereotyped LLR includes the P1¹, N1, P2, and N2 components, which typically span
170 approximately 50 to 300 ms, following sound onset (Davis and Zerlin 1966; Davis 1939;
171 Vaughan and Ritter 1970). A variety of sounds, including clicks (e.g., Arslan et al. 1984), tones
172 (e.g., Davis and Zerlin 1966), and speech sounds (e.g., Kraus et al. 1993), can be used to elicit
173 the LLR. The primary and non-primary auditory cortices, with contributions from the association
174 and possibly frontal cortices, are the putative generators of the LLR (Hari et al. 1980; Kanno et
175 al. 2000; Naatanen and Picton 1987; Picton et al. 1999; Scherg and Von Cramon 1985; Shahin
176 et al. 2007; Vaughan and Ritter 1970).

177 A fourth measure of auditory function that our paradigm was designed to elicit is the
178 ASSR (also known as the 40 Hz Response) (Galambos et al. 1981). Transient stimuli (e.g.,
179 clicks or tones) that repeat at a constant rate (often ~40 Hz, or every ~25 ms, in the auditory
180 domain), or amplitude-modulated tones or noise can lead to a sinusoidal-shaped event-related
181 potential (ERP), also known as a steady-state response (for a review, see Korczak et al. 2012;
182 Picton et al. 2003)². Generally, the ASSR is analyzed in the frequency domain (via a Fourier
183 transform) or time-frequency domain (e.g., via wavelet decomposition), so that amplitude peaks
184 at the stimulation frequency and its harmonics are clearly visible (e.g., Artieda et al. 2004;
185 Stapells et al. 1984). Regarding the neural generators of the ASSR, taken together, MEG and
186 EEG studies have demonstrated that both the auditory brainstem and auditory cortex contribute
187 to the 40-Hz ASSR (e.g., Makela and Hari 1987; Ross et al. 2002; Schoonhoven et al. 2003;
188 Coffey et al. 2016; Herdman et al. 2002).

189 **Visual Responses**

190 The current paradigm was also designed to elicit onset visual evoked potentials (VEPs)
191 and the steady-state visual evoked potential (SSVEP). The onset VEP generally consists of the

192 P1, N1, and P2 components, which can be evoked by a variety of visual stimuli, including
193 flashes, checkerboard, or grating stimuli. The VEP complex is evident from approximately 50 to
194 250 ms after visual stimulus onset (e.g., Clark et al. 1994; Jeffreys and Axford 1972). Many
195 studies have localized the P1 and N1 to extrastriate regions (e.g., Clark et al. 1994; Di Russo et
196 al. 2002; Gomez Gonzalez et al. 1994), but both striate and extrastriate regions may contribute,
197 at least to the P1 (Aine et al. 1995; Di Russo et al. 2005; Vanni et al. 2004). The generators of
198 the visual P2 are not well understood and likely involve multiple cortical sources (Clark et al.
199 1994). However, the P2 has been shown to peak over the vertex following both auditory and
200 visual stimuli, suggesting that neurons in amodal cortical regions may contribute to both auditory
201 and visual P2 responses (Perrault and Picton 1984).

202 Unlike onset VEPs, which are transient onset responses, SSVEPs are brain responses
203 to a flickering visual stimulus that has a constant flicker rate, such as sinusoidally-modulated
204 flashes of light (Regan 1966; Van Der Tweel and Lunel 1965) or checkerboards in which the
205 black checks change to white and vice versa at a constant rate (e.g., Burkitt et al. 2000; Thorpe
206 et al. 2007). SSVEPs have a spectral amplitude distribution that remains stable over time and
207 reflects the visual stimulus' flicker rate (and its harmonics); thus, instead of analyzing SSVEPs
208 in the time domain, they are generally analyzed in the frequency domain, using a Fourier
209 transform, or in the time-frequency domain (e.g., using a wavelet approach) (for reviews, see
210 Norcia et al. 2015; Regan 1977; Vialatte et al. 2010). One observation critical to the design of
211 the current paradigm is that multiple visual stimuli with different flicker rates can be presented
212 concurrently to “frequency-tag” neural activity, in other words, to isolate SSVEPs for each
213 separate stimulus/rate presented (e.g., Andersen et al. 2008; Ding et al. 2006; Itthipuripat et al.
214 2013; Keitel et al. 2010; Muller et al. 2003; Regan and Heron 1969).

215

216 **Expected Findings.**

217 We anticipated that the ABR, MLR, LLR, and ASSR, as well as the VEP and SSVEP,
218 would be reliably detected in all individuals. Previous studies which used long-duration auditory
219 stimuli (Krishnan et al. 2012; Picton et al. 1978a; b) showed that the resulting LLR does not
220 have canonical P1-N1-P2 morphology, but rather it has a broad P1, followed by an N1 and a
221 sustained negativity. Thus, since the present paradigm employs continuous speech stimuli, we
222 expected similar non-canonical morphology as shown in the aforementioned studies.

223 **Materials and Methods**

224 **Participants**

225 Twenty-six healthy young adult volunteers participated in this study; however, due to
226 technical problems during one participant's session, data from 25 participants were analyzed
227 (14 females, Age Range: 18 to 28 years, Mean Age: 21 years; one participant did not provide
228 his age). Participants were right-handed, fluent English speakers, who self-reported normal
229 hearing, normal or corrected-to-normal visual acuity, normal color vision, no history of any
230 neurological illnesses, and no known problems with speech or reading. All participants gave
231 informed written consent before commencing the study, and the UC Davis Institutional Review
232 Board approved all procedures described herein.

233 **Visual Stimuli**

234 As illustrated in **Figure 1A**, the visual stimuli included a cartoon played in the middle of
235 the screen, surrounded by two concentric checkered rings. The cartoon serves as an engaging
236 event and is designed to help control a participant's fixation. For this study, we used a variety of
237 cartoon clips and videos of animals that were gleaned from the internet and compiled and edited
238 using Final Cut Pro software (Apple, Inc.). These video clips were selected for subsequent

239 testing of elementary school-aged children. We took care to avoid or edit out portions of
240 cartoons which involved characters talking, to prevent any attempts to audio-visually integrate
241 the cartoon and the Cheech. The inner ring comprised eight equally-spaced checks, which
242 flickered sinusoidally at a rate of 7.5 Hz. The outer ring comprised 16 equally- spaced checks,
243 which flickered sinusoidally at 12 Hz. To prevent the flickering from being overly bothersome to
244 participants, the rings flickered for 2.5 seconds, and then stopped for 1-3 seconds (randomly
245 jittered, rectangular distribution), before the flickering began again. In each ring, alternate
246 checks flickered in counter-phase, as depicted in **Figure 1A**. Additionally, within each ring and
247 between every flickering check was a “blank” check or gap, the same color as the background,
248 which did not flicker; this was done to prevent multiple checks stimulating a given location on
249 the retina, as eye movements naturally occur during cartoon viewing. In this way, since no
250 adjacent checks flicker out of phase, no retinal location receives phase-opposed stimulation
251 over time during small eye movements.

252 The visual stimuli were created using MATLAB (The MathWorks, Inc.,
253 <https://www.mathworks.com/>), and the cartoon and flickering rings were embedded into six 2-
254 minute videos (AVI files). Participants sat 32 inches (~81.28 cm) from the monitor. The spacing
255 between checks (angular distance), as well as the radial spacing between rings was chosen
256 such that it was approximately half the cartoon width – again to avoid multiple checks
257 stimulating the same retinal location. The cartoon extended $\sim 2.7^\circ$ (visual angle) to the left and
258 right of screen center ($\sim 5.5^\circ$ total cartoon width), and $\sim 1.8^\circ$ (visual angle) above and below
259 screen center ($\sim 3.66^\circ$ total cartoon height). The inner edge of the inner ring was adjacent to the
260 border of the cartoon (see **Figure 1**), and the inner ring’s outer edge subtended a visual angle
261 of $\sim 5.8^\circ$ from screen center, while the inner edge of the outer ring was $\sim 10.1^\circ$ from screen
262 center. The outer ring was made larger than the inner ring to approximately account for cortical
263 magnification (Cowey and Rolls 1974; Daniel and Whitteridge 1961). The individual checks of

264 the outer ring extended to varying visual angles from screen center, according to the boundaries
265 of the screen edge. For example, at the corners of the screen (longest distance from screen
266 center), the outer ring extended to a visual angle of $\sim 20.5^\circ$, whereas at the shortest distance
267 from screen center (top or bottom of the screen, directly above or below screen center,
268 respectively), the outer ring extended to a visual angle of $\sim 11.3^\circ$. The cartoon was rendered at
269 147 x 98 pixels and combined in MATLAB with the flickering ring stimuli which extended 960 x
270 600 pixels. Upon stimulus delivery via Presentation software (Neurobehavioral Systems, Inc.,
271 <https://neurobs.com>), which doubled the video size, the cartoon resolution was 294 x 196 pixels
272 and the full video resolution was 1920 x 1200 pixels.

273 We originally manipulated the color/luminance of the checks to determine the paradigm's
274 sensitivity to changes in color/luminance. In one block (three 2-minute videos per block), the
275 checks were black and white against a gray background (RGB color components: [0 0 0]; [255
276 255 255]; [128 128 128], respectively); in the other block, the checks were red and green,
277 against a mustard yellow background (RGB color components: [255 0 0]; [0 255 0]; [128 128 0],
278 respectively). Block order was counterbalanced across participants. The flickering involved
279 luminance changes between black and white or color changes between red and green (the gray
280 and yellow intervening gaps did not change). Rather than using abrupt luminance or color
281 transitions, a sinusoidal function was applied, such that the speed of the transition depended on
282 the screen's refresh rate (60 Hz) and the flicker rate. Thus, for the inner ring (7.5 Hz flicker), the
283 color/luminance transition occurred gradually across eight frames (i.e., screen refreshes), while
284 for the outer ring (12 Hz flicker), the transition occurred across five frames. During each block,
285 there were 90 2.5-second intervals, in which the checkered rings were flickering. The EEG data
286 were time-locked to these flicker onsets to compute the visual onset responses and SSVEPs.
287 The two visual color conditions (black-white, red-green) were not isoluminant, thereby

288 confounding interpretations about any differences observed between color conditions. Thus, we
289 collapsed across black-white and red-green trials for EEG data analysis.

290 **Auditory Stimuli**

291 **Figure 1B** shows an example of the auditory stimuli. A detailed characterization of
292 these auditory stimuli (termed CHirp-spEECH, “Cheech”) can be found in the patent listing
293 (Miller et al. 2017). Unlike fully natural speech, Cheech possesses acoustic properties that
294 robustly drive early (ABR) as well as middle and late auditory EEG responses. As implied in its
295 name, Cheech incorporates auditory chirp stimuli; chirps are transient sounds that increase
296 rapidly in frequency over time. Furthermore, Cheech takes advantage of the observation that
297 upward frequency-modulated chirps yield more synchronized brainstem responses than
298 traditional stimuli such as clicks, by compensating for the traveling wave delay (across
299 frequencies) along the basilar membrane (Dau et al. 2000; Elberling et al. 2007; Shore and
300 Nuttall 1985). In Cheech, we replace some of the glottal pulse energy with chirp energy,
301 thereby yielding stronger speech EEG responses. Briefly, 49 unique sentences (sampled at
302 22,050 Hz) from the Harvard/IEEE Corpus (1969) were selected and concatenated into a two-
303 minute WAV file of continuous speech. Next, the pitch of the voicing was flattened to 82 Hz
304 using Praat (Boersma and Weenink 2001, <http://www.praat.org/>). A second sound was then
305 created with trains of chirps temporally coinciding with each voiced period, such that the
306 individual chirps were aligned in time with individual glottal pulses in the speech (i.e., every
307 other glottal pulse). Voiced periods with coinciding chirps occurred whenever the speech
308 envelope <40Hz for energy between 20-1000Hz (containing the highest voiced power)
309 surpassed a threshold (appx. 28% of overall speech RMS) long enough to contain four chirps
310 total. Finally, the speech and chirps were frequency multiplexed in alternating, interleaved
311 bands one octave wide and added together (speech energy occupied [0 250], [500-1000],
312 [2000-4000] Hz, and chirp energy occupied [250-500], [1000-2000], [4000 10,000] Hz). In this

313 way, chirps align acoustically and perceptually with the natural voicing, creating a single
314 perceptual speech object. Chirps occurred at a rate of 41 Hz within each voiced period, to elicit
315 the ASSR at 41 Hz. Furthermore, the chirps were isochronous throughout the WAV file (due to
316 the flattened pitch), so that each chirp occurred at multiples of ~24 ms, relative to the first chirp
317 in each experimental block. Within each voiced period, the second chirp was omitted, in order
318 to measure an MLR that occurred in response to the onset of the voiced period (which coincides
319 with the first chirp). The voicing periods occurred on average 501 ms apart (range: 146 to 1195
320 ms apart) in the present study. The resulting stimulus is highly intelligible speech, albeit with a
321 robotic monotone quality; the rapid interspersed chirps are audible as a rattling character in the
322 voicing, but they blend perceptually with the speech and do not distract from its linguistic
323 content.

324 Across both 6-minute blocks, there were 1,422 voicing onsets (711 per block) and
325 11,694 chirps (5,847 per block). As we demonstrate here, using Cheech in conjunction with
326 EEG, robust measurements of auditory responses along the entire auditory pathway, from the
327 brainstem to auditory cortex, can be obtained (Miller et al. 2017). Specifically, ABRs can be
328 created by time-locking and signal averaging the continuous EEG data, relative to the onset of
329 each chirp. By time-locking the EEG data to the onsets of the voicing periods, MLRs, LLRs, and
330 ASSRs can be measured.

331 In this study, the two-minute WAV file of Cheech was repeated three times within each
332 of the two blocks. The Cheech was presented in the free-field at a level of 65 dB(C) SPL, using
333 an internal Realtek HD sound card, a NuForce Icon stereo amplifier, and finally played through
334 an Auvio 400016 speaker (passive speaker, three drivers in speaker chassis) that was
335 positioned 1.27 m directly in front of the participant and above the computer screen. Previously,
336 Cheech has been presented monaurally (Miller et al. 2017), but we chose to use the free-field
337 approach because of our intention to use this paradigm in children with cochlear implants. A

338 sample stimulus video, which includes the Cheech audio, can be accessed online here:
339 [https://figshare.com/articles/Novel EEG Paradigm J Neurophysiology Methods Backker et al](https://figshare.com/articles/Novel_EEG_Paradigm_J_Neurophysiology_Methods_Backker_et_al_2019pptx_pptx/8214449)
340 [_2019pptx_pptx/8214449](https://figshare.com/articles/Novel_EEG_Paradigm_J_Neurophysiology_Methods_Backker_et_al_2019pptx_pptx/8214449).

341 **Electroencephalography (EEG) Recording**

342 EEG data were recorded using a BioSemi ActiveTwo system (BioSemi B.V.,
343 Netherlands, biosemi.com), a 32-channel cap, and ActiView2 software installed on a Dell laptop.
344 The scalp electrode montage (based on the International 10/20 System) included: FP1/2, AF3/4,
345 Fz/3/4/7/8, FC1/2/5/6, Cz/3/4, T7/8, CP1/2/5/6, Pz/3/4/7/8, PO3/4, Oz/1/2. Additional
346 electrodes were taped to each earlobe and each mastoid. EEG data were sampled at a rate of
347 16,384 Hz in order to obtain ABRs, which require sub-millisecond resolution; an anti-aliasing
348 low-pass filter at 3,334 Hz (5th order sinc) was applied before A-to-D conversion. Before
349 beginning the recording, electrode offsets (relative to the Common Mode Sense (CMS)
350 electrode) for all channels were set to < 20 μ V.

351 During EEG recording, the visual and auditory (Cheech) stimuli were simultaneously
352 presented using Presentation software, from a Dell laptop to a 24-inch HP Z Display monitor
353 and to the speaker inside the testing room. The EEG recording lasted for a total time of 12
354 minutes (6 minutes per block). Participants were instructed to focus on the cartoon, with no
355 explicit instruction to ignore the flickering visual or the Cheech stimuli. As mentioned previously,
356 the inter-stimulus interval for the visual flicker stimuli was jittered from one to three seconds,
357 while the cartoon was played continuously; however, the Cheech was looped without any silent
358 periods. Thus, there were periods within each block, in which the participants experienced only
359 Cheech and no visual flickers (auditory-only); at other times, both the flickers and the Cheech
360 were concurrent (audio-visual) (**Figure 1C**). All auditory events (i.e., during both the auditory-

361 only and audio-visual periods) were used in computing the auditory EEG responses reported
362 here.

363 **EEG Data Analysis**

364 ***Preprocessing.***

365 EEG data were preprocessed in MATLAB, using EEGLAB (Delorme and Makeig 2004),
366 ERPLAB Toolbox (Lopez-Calderon and Luck 2014), and custom MATLAB code. First, raw data
367 (BDF files) were imported into EEGLAB using the BioSig plugin (version 2.88,
368 <https://sourceforge.net/projects/biosig/>).

369 During EEG acquisition, experimental events were synchronized with the EEG data
370 using parallel port codes, sent from the presentation computer, using a StarTech IEEE 1284
371 parallel port card, to the Biosemi acquisition box. For the visual stimuli, a single port code was
372 sent via Presentation software at the onset of each 2-minute video; but the time stamp
373 corresponding to the onsets of the flicker interval within each video were added post-hoc,
374 relative to each video onset, using custom MATLAB code. Since the videos were created in
375 MATLAB, the exact frames corresponding to the start of the flicker interval were known in
376 advance. Using Presentation's detailed logging feature for videos, we obtained information
377 about the onset time for each frame, the uncertainty about each frame's onset time (usually 1-2
378 ms), and the number of frames dropped for each participant (usually no frames dropped).
379 Furthermore, using a photodiode and oscilloscope, we checked the timing between the delivery
380 of the EEG port code at the start of each video and the actual start of the video to ensure
381 reliable timing.

382 For the auditory stimuli, Presentation sent one port code at the beginning of each WAV
383 file, as well as port codes for all of the Cheech events of interest (i.e., voicing onsets and
384 chirps). These were all embedded as metadata within the WAV files and were sent by

385 Presentation at appropriate latencies as the WAV files played. It is important, particularly for
386 ABR analyses, to ensure accurate sub-millisecond precision between the port code times and
387 when the Cheech events of interest actually played; however, in our system, comparing the
388 sound output and port output using an oscilloscope, the port code timing variability was too
389 great for ABR analyses (~1 ms jitter). In addition, port codes were frequently missed due to the
390 unusually high load for the parallel port in sending codes every ~24 ms. Many acquisition
391 systems would not suffer these limitations, as they provide an additional data channel dedicated
392 to timing pulses aligned precisely with the stimuli (further described in the Discussion).
393 However, in our own system, a crucial step involved developing MATLAB code to correct these
394 timing issues, particularly for the ABRs. Thus, we conducted a cross-covariance analysis
395 between the recorded port codes in the EEG data and the intended port codes embedded in the
396 WAV file metadata (taking into account the difference in sampling rates between the WAV files
397 and EEG recordings). This yields large covariance peaks at the onset of each WAV file, which
398 we then used as a temporal reference to replace all recorded port codes with reconstructed
399 ones from the WAV files themselves. Thus, the event timing used in the analyses has
400 essentially no variability due to port code timing errors. An analysis of the timing difference
401 between the recorded port codes and the reconstructed port codes revealed that 8.95% of the
402 original, recorded auditory port codes were jittered by more than 0.2 ms.

403 One further temporal correction was necessary, due to the fact that experimental
404 devices may differ slightly in how they measure time. Thus, over long recording periods, the
405 stimulus presentation computer or sound card can nominally drift out of sync from the EEG
406 acquisition device. Put in another way, reported time runs slightly slower or faster for different
407 devices. This required us to compress time for the target port codes by a very small percentage
408 (0.003%) to accommodate the difference.

409 Due to divergent analyses after the addition/correction of port codes, the various
410 preprocessing pipelines are described separately below.

411 Auditory LLRs and Visual Responses.

412 Following port code addition/correction, the data were resampled to 512 Hz, and each
413 block's data was concatenated. Next, the data were inspected visually across the entire
414 recording, noisy data segments were removed, and bad channels were noted. Each
415 participant's data were referenced to the average earlobes, and band-pass filtered from 0.5 to
416 100 Hz, using an 8th order, zero-phase Butterworth filter. The DC offset of contiguous segments
417 of data was removed prior to filtering, in order to minimize edge effects at boundaries. One
418 participant's data was also filtered using a Park's-McClellan notch filter (order of 180) to remove
419 60 Hz noise. The filtered data were then processed with EEGLAB's Independent Component
420 Analysis (ICA) function, which used the Infomax algorithm (Bell and Sejnowski 1995); the
421 reference (earlobe) channels, as well as any bad channels, were excluded from ICA. The
422 components were visually inspected, and only eye blink components were removed from the
423 data; twenty-three participants had one component removed, and two participants had two
424 components removed. For the data used to create visual onset ERPs, as well as the auditory
425 long latency responses, the data were down-sampled further to 256 Hz. Next, any bad
426 channels identified previously were spatially interpolated using a spline function; ten participants
427 had no bad channels, six had one bad channel, five had two bad channels, two participants had
428 three bad channels, and two participants had five bad channels.

429 *Filtering and Epoching.* The next steps occurred in the same order for each participant's data,
430 however, the filter and epoch settings differed depending on the type of response that was
431 being extracted, as detailed below. Following interpolation of bad channels, the data were
432 filtered with an appropriate zero-phase, 8th order Butterworth filter to obtain the desired

433 passband for each response type. For the VEP onset response and the auditory LLR, the data
434 were low-pass filtered with a 30 Hz cutoff frequency, resulting in a passband of 0.5 to 30 Hz.
435 The SSVEP was analyzed in the frequency domain (using a Fourier transform). For the SSVEP
436 response, a band-pass filter was applied with cutoffs at 1 and 40 Hz. Next, using ERPLAB
437 Toolbox, information about the time-locking events of interest (e.g., flickering onsets) was
438 obtained, and the data were epoched and baselined to the pre-stimulus data. The epoch limits
439 differed according to response type as follows: Auditory LLR: -50 to +500 ms; VEP Onset
440 Response: -100 to +500 ms; SSVEP: -500 to +2500 ms. In general, the baseline length was
441 selected to be proportional to the post-stimulus epoch length. For the VEP and SSVEP, the
442 baseline length corresponded to 20% of the post-stimulus epoch time. A relatively short pre-
443 stimulus baseline (50 ms) was used for the Auditory LLR due to the continuous nature of the
444 Cheech, to minimize contamination of previous auditory responses on the current epoch's
445 baseline. Both the Auditory LLR and VEP Onset Response epochs included 500 ms of post-
446 stimulus data, to ensure analysis of all transient ERP components, as well as the sustained
447 negativity observed in the LLR. The SSVEP epoch included data samples for the entire
448 duration of the flickering visual stimulus, which lasted 2.5 seconds. All visual response analyses
449 were time-locked to the start of each 2.5-second flickering stimulus, and the LLRs were time-
450 locked to the voicing onsets in the Cheech, specifically the first chirp in each voiced period.

451 *Voltage Threshold Artifact Rejection.* Next voltage threshold artifact rejection was done, based
452 on the whole epoch length in all channels except for T7/8, earlobe, and mastoid channels; this
453 excluded any epochs with deflections exceeding $\pm 80 \mu\text{V}$ from further analysis. This
454 thresholding procedure resulted in the following across-subjects mean percent and mean
455 number of accepted epochs and the across-subjects range of number of accepted epochs, for
456 each response type and visual condition: Auditory LLR: 97% accepted, 1369 mean epochs,

457 1185-1422 epochs; Visual Onset: 98%, 174 epochs, 152-180 epochs; SSVEP: 96%, 171
458 epochs, 139-180 epochs.

459 MLRs and ASSRs.

460 Following port code correction/addition, noisy segments within the continuous data were
461 removed, corresponding to the same latencies as those excluded for the auditory LLRs and
462 visual response analyses. Next, the data were resampled to 1024 Hz, referenced to the
463 average earlobes, and filtered using a zero-phase, band-pass (0.5 to 200 Hz), 8th order
464 Butterworth filter (DC offset was removed prior to filtering). One subject's data were also notch-
465 filtered to remove 60 Hz noise, as previously described. The Independent Component weight
466 matrix calculated for the visual response/auditory LLR analysis stream was applied to the
467 current analysis as well, and the same eye blink component(s) that were removed for the
468 visual/LLR data were also removed from each subject's MLR/ASSR dataset. Next, any bad
469 channels were spatially interpolated (same channels as for the visual/LLR data), and the data
470 were high-pass filtered with a cut-off frequency of 15 Hz using a zero-phase, 8th order
471 Butterworth filter, resulting in a passband of 15 to 200 Hz for the MLR/ASSR data. At this point,
472 the auditory port codes were shifted in time to account for the time it takes for sound to travel
473 1.27 m, from the speaker to the participant (~ 3.7 ms). Next, ERPLAB was used to extract
474 information about the voicing onsets, to which the MLRs and ASSRs were time-locked, and the
475 data were epoched and baselined to the pre-stimulus data. The epoch time limits were as
476 follows: MLR: -5 to +60 ms; ASSR: -150 to +1100 ms. For the MLR, these epoch time limits
477 were originally chosen to encapsulate the entire MLR; recall that there was a 48.8-ms gap
478 between the voicing onset/chirp to which the MLR was time-locked and the next chirp. Like the
479 LLR and ABR, a relatively short baseline period (5 ms) for the MLR was chosen to minimize
480 contamination from residual neural activity due to the continuous auditory stimuli. The ASSR
481 baseline length (150 ms) was selected as a compromise between the long duration of the post-

482 stimulus epoch length and the need to minimize contamination of the baseline due to the
483 continuous Cheech stimuli. Finally, voltage threshold artifact rejection was done, as previously
484 described, excluding any epochs with deflections exceeding $\pm 80 \mu\text{V}$ from the ERP averages.
485 This resulted in the following mean percent and mean number of accepted epochs, and range
486 across subjects: MLR: 97% of epochs accepted on average, 1369 mean epochs, 1180-1422
487 epochs; ASSR: 92% of epochs accepted, 1294 mean epochs, 967-1419 epochs.

488 ABRs.

489 For the ABRs, following port code addition/correction, the EEG data files for each block
490 were then concatenated into one file. Noisy data segments, corresponding to the same
491 latencies as those excluded for the other visual and auditory data, were removed. The data
492 were referenced to the average earlobes, and any bad channels were spatially interpolated with
493 a spline function. These bad channels were the same as those identified in the other auditory
494 and visual data. Next, the data were filtered, using a band-pass (100 to 1500 Hz) Butterworth
495 filter (order of 8), and the chirp port codes were shifted in time to account for sound travel time
496 from the speaker to the participant. ERPLAB toolbox was then used to obtain chirp onsets,
497 epoch the data to time-lock to them (epoch limits: -2 to 24 ms) and to baseline the data to the
498 pre-stimulus period. The epoch limits were chosen because there was a minimum of ~ 24 ms
499 between chirps, and a brief pre-stimulus baseline (2 ms) was used to minimize contamination
500 from residual brainstem activity due to the continuous Cheech stimuli. Threshold artifact
501 detection was conducted to identify and exclude epochs in which activity exceeded $\pm 35 \mu\text{V}$, in a
502 subset of channels. ICA was not done for the ABR ERPs, since the ABR passband of 100 to
503 1500 Hz removes most, if not all of the eye blink artifact. Because the ABR signal is small in
504 comparison to muscle activity and since the ABR peaks at the vertex (Cz), channels near the
505 forehead and temples (which tend to have the most muscle activity) including FP1/2, AF3/4,
506 F7/8, as well as any bad channels and the earlobe and mastoid channels, were excluded from

507 threshold artifact detection; this was done to preserve as many epochs as possible, with clean
508 EEG signals in the central channels of interest, for creating the ABRs. This resulted in the
509 preservation of an average of 90% of epochs (mean = 10428 epochs, range = 6967-11640
510 epochs) across subjects.

511 ***Statistical Analyses.***

512 Custom MATLAB code was used for statistical analysis of the EEG data. Since the goal
513 of this study was to validate the EEG paradigm at the single-subjects level, statistics were run
514 on each individual subject's data, using a bootstrapping approach based on Zhu et al. (2013).
515 This allowed us to quantify the number of subjects that exhibited significant responses to the
516 auditory and visual stimuli. The bootstrapping algorithm differed slightly for different responses,
517 as described below.

518 ABRs, MLRs, LLRs, and VEPs.

519 For each subject, the preprocessed, epoched data were imported into MATLAB. For the
520 ABRs and MLRs, the data epochs were shortened to -2 to +15 ms and -5 to +53 ms,
521 respectively. For the ABR, this was done primarily to speed-up computation time of the
522 statistical analysis, since the components of interest occurred within 15 ms. Furthermore, the
523 original MLR epoch included additional time points to +60 ms; however, because the next chirp
524 always occurred at approx. +48.8 ms, the original MLR included the ABR Wave V to the
525 subsequent chirp. Thus, the MLR was truncated to +53 to encompass the Pb and exclude the
526 subsequent Wave V. Pre-stimulus time points were included in the ERP Bootstrapping analysis
527 and are shown in the results figures; this was done for transparency and to ensure that no
528 robust responses were observed due to the continuous nature of especially the auditory
529 stimulus. To generate an estimate of the actual data, a subset of epochs was randomly selected
530 with replacement and the average of this data subset was computed, resulting in an ERP in

531 each of the 32 scalp channels (excluding earlobe and mastoid channels). This was repeated
532 100 times, and the grand average of these 100 draws was computed.

533 To create the null distribution, a subset of actual data epochs was randomly selected
534 with replacement and the amplitude values comprising each epoch were randomly scrambled in
535 time. The mean of these scrambled data epochs was computed. These steps (i.e., draw,
536 scramble, average) were repeated 100 times, and the grand average of these 100 draws was
537 computed. This full process was iterated 1,000 times to generate the null distribution. Since
538 creating the null distribution is computationally expensive, we limited the creation of the null
539 ERPs to only one or two channels as follows: Cz for ABRs, Fz and Cz for MLRs and LLRs, and
540 Oz for VEPs. These channels were chosen based on *a priori* knowledge of the scalp regions
541 where auditory and visual evoked responses generally reach their peak amplitudes (Luck and
542 Kappenman, 2011). The null ERPs were then filtered, using the same filter parameters as done
543 on the actual data, and then baselined to the pre-stimulus period. Each subject's data was used
544 to generate their own null ERPs.

545 Each individual's null distribution was used to statistically test their own actual data. To
546 control for multiple comparisons across channels and time points, the maximal absolute null
547 value across channels and time points was recorded, resulting in a vector with 1,000 maximal
548 null values. This vector was then sorted in descending order. Next, the absolute value of each
549 actual data point was compared to the sorted maximal null vector, to determine the proportion of
550 null samples that were larger than the absolute value of the actual data point (i.e., resulting in its
551 p-value). This was repeated for each subject and response. Because the maximal null vector
552 comprised 1,000 samples, the minimum p-value possible was 0.001, which was used as the
553 threshold for the single-subject results.

554 To determine the number of participants with significant responses for each ERP
555 component, we first plotted the group average ERPs and found the peak latency for each
556 observed positive and negative deflection in Channel Cz for ABR, Fz for MLR and LLR, and
557 channel Oz for VEP. Next, using custom MATLAB code, an automated procedure scanned
558 individual subjects' data to ascertain the number of data samples that reached a p-value of
559 0.001 within a window around the group mean peak for that particular component. The window
560 was defined as the group-mean latency \pm 1, 3, or 20 ms for the ABR, MLR, or LLR/VEP
561 responses, respectively. These window durations were chosen in accordance with *a priori*
562 knowledge of the duration of each component peak and confirmed via inspection of the group-
563 averaged ERPs in the present study. Thus, we selected the window durations to account for
564 the increase in peak width from the ABR to MLR to LLR. Since both the VEP and LLR are
565 cortical responses with relatively broad peaks (compared to ABRs and MLRs), we chose a
566 window size of \pm 20 ms for consistency in the analysis of both types of cortical responses. For
567 sustained cortical responses (i.e., LLR sustained negativity and VEP late negativity), the window
568 was defined according to the duration of the group-average sustained response. A single-
569 subject significant response was defined as follows: the number of data samples that deflected
570 in the correct direction (positive or negative) and reached a p-value of 0.001 had to exceed one-
571 third of the number of total data samples in the specified window.

572 SSVEPs and ASSRs.

573 First, an estimate of the real data was obtained by drawing randomly with replacement, a
574 subset of data epochs. Next, each selected epoch was converted to the frequency domain via a
575 Fast Fourier Transform (FFT) applied from 50 to 1050 ms of the ASSR epochs (i.e., 1 Hz
576 resolution) and from 500 to 2500 ms of the SSVEP epochs (i.e., 0.5 Hz resolution, since the
577 inner ring flickered at 7.5 Hz). For the ASSR, we extracted the data samples starting at 50 ms
578 to avoid the transient portion of the onset response, which arises primarily from subcortical

579 structures and comprises broadband spectra that overlaps with the ASSR. Likewise, for the
580 SSVEP, we used the data samples starting at 500 ms to avoid the visual onset response,
581 whose spectral energy overlaps with that of the flicker rates. The single-sided FFT was
582 computed for each epoch and scaled to the number of data samples on which the FFT was
583 performed. The mean single-sided FFT (complex-values) was computed across the subset of
584 data epochs drawn, and the absolute value was taken to obtain magnitude. These magnitude
585 values were then converted to dB (arbitrary units). This procedure was repeated 100 times (i.e.,
586 number of draws), and the grand average magnitude was calculated across these 100 draws to
587 obtain the estimated magnitude of the actual data in each of the 32 scalp electrodes. This was
588 repeated for each participant's data.

589 To create the null distribution for each participant, the same steps were followed for the
590 actual data. However, after computing the FFT for each epoch, the magnitude component of
591 the FFT was preserved, but the phase was randomized from 0 to 2π . In theory, this should
592 provide an accurate estimate of the noise floor in the data (Zhu et al. 2013). Thus, phase-
593 randomized FFTs were obtained, using the actual data's magnitude component and the random
594 phase vector. Next, just like the actual data, the phase-randomized FFTs were converted to the
595 single-sided spectra, scaled, and averaged across epochs. The magnitude component was
596 extracted and converted to dB (arbitrary units). The grand average dB magnitude was
597 computed across 100 draws, and this whole procedure was repeated 1,000 times to create the
598 null (phase-randomized) distribution. Due to the computational cost of creating the null
599 distribution, this was limited to channels Fz and Cz for the ASSRs and to channel Oz for the
600 SSVEPs. Like the ERP analysis, these channels were chosen based on *a priori* knowledge of
601 the scalp regions where auditory and visual evoked potentials generally reach their peak
602 amplitudes (Luck and Kappenman, 2011). For data visualization, the signal-to-noise ratio

603 (SNR) was obtained by subtracting the mean of the null distribution (i.e., the noise floor, in dB
604 units) from the mean of the estimated actual data (in dB units), for each participant.

605 Statistics were performed at the single-subjects level. For each channel (Fz and Cz, or
606 Oz) and frequency of interest (i.e., ASSR: 41 Hz (f_0), 82 Hz, 123 Hz, 164 Hz; SSVEP: 7.5 Hz
607 (Inner ring f_0), 12 Hz (Outer ring f_0), 15 Hz (Inner ring harmonic), 24 Hz (Outer ring harmonic)),
608 the actual data value was compared to the distribution of null values at that frequency to
609 determine its p-value. A Bonferroni-corrected threshold was computed as $0.05/(f*c)$, where f is
610 the number of frequencies of interest (i.e., 4) and c is the number of channels examined (i.e., 2
611 for ASSR, 1 for SSVEP), resulting in thresholds of 0.00625 for ASSR and 0.0125 for SSVEP.
612 These Bonferroni-corrected thresholds were used to determine the number of subjects with a
613 significant response at each frequency of interest.

614 Number of Epochs for Bootstrapping.

615 The number of epochs drawn for each response type was initially based on the minimum
616 number of epochs available after artifact rejection across subjects, so that all subjects could be
617 included in all analyses. These epoch numbers were further reduced, to accommodate the
618 minimum number of artifact-free trials that we expect (and have obtained) from young children
619 participating in the same EEG paradigm. For all visual responses (VEP, SSVEP), 50 epochs
620 were drawn (randomly, with replacement) for each iteration of the bootstrapping analysis. For
621 all auditory responses (ABR, MLR, LLR, and ASSR), 500 epochs were selected (randomly, with
622 replacement).

623 Assessing Relationships among Auditory and Visual EEG Responses.

624 As a supplementary analysis, we conducted across-subjects correlations to determine if
625 the various auditory and visual EEG responses varied in a systematic way. To do this, we
626 converted the amplitude estimates of a subject's true data for each EEG response into z-scores,

627 relative to the mean and standard deviation of each subject's null distribution. For each ERP
628 response, each subject's null distribution mean and standard deviation were computed across
629 all time points and channels for which the null was computed. For the steady-state responses,
630 each subject's null distribution mean and standard deviation were computed using the one or
631 two channels for which the null was created, but separately for each frequency of interest. By
632 converting the data to z-scores, we could directly compare different responses with different
633 magnitudes or measurement units (see also Zhu et al. 2013). For the ERP responses (ABR,
634 MLR, LLR, VEP), each individual's peak z-score was obtained for each component, using the
635 same windowing procedure as described for quantifying the number of subjects with a
636 significant ERP response. Data from one channel were used from each EEG response: Cz for
637 ABR, Fz for MLR, LLR, and ASSR, and Oz for VEP and SSVEP. For any observed sustained
638 potentials, each individual's z-scores across the time range of the group-mean sustained
639 potential were averaged. Next, the negative components' z-scores were multiplied by -1, and
640 the z-scores corresponding to each component within a given response were averaged (e.g.,
641 P1, N1, and sustained negativity for LLR). This was done to create an aggregate z-score for
642 each EEG response. Similarly, for the ASSR and SSVEP, the z-scores corresponding to each
643 frequency of interest were averaged.

644 Using MATLAB, Pearson correlations (two-tailed) were conducted across-subjects for
645 each possible pair of auditory responses (ABR-MLR, ABR-LLR, ABR-ASSR, MLR-LLR, MLR-
646 ASSR, and LLR-ASSR) and between the visual responses (VEP-SSVEP). Also, to assess if the
647 frequencies of interest were correlated within the ASSR and SSVEP responses, pairwise
648 Pearson correlations were computed on the z-scores of each frequency of interest (ASSR: 41-
649 82 Hz, 41-123 Hz, 41-164 Hz, 82-123 Hz, 82-164 Hz, 123-164 Hz; SSVEP: 7.5-12 Hz, 7.5-15
650 Hz, 7.5-24 Hz, 12-15 Hz, 12-24 Hz, 15-24 Hz).

651

652

Results

653 ERP Responses (ABR, MLR, LLR, VEP)

654 **Table 1** contains a summary of the number of subjects showing a significant response
655 for each observed component, along with peak amplitude and latency measurement results.

656 Examination of the ABR data revealed two negative peaks interleaved with two positive
657 deflections (**Figure 2**). The first negative peak, which we have labeled “ n_0 ”, occurred around 3.5
658 ms and was maximal over fronto-central channels (significant for 24 subjects). Next, we
659 observed a positive peak at 6.5 ms, which was maximal over the vertex, consistent with the
660 timing and topography of Wave V (significant for all 25 subjects). Another negative peak
661 followed around 9 ms (significant for all 25 subjects), and a positive peak at 13 ms, which were
662 maximal over frontal sites, suggesting a neural generator in/near auditory cortex. These peaks’
663 timings are consistent with the N_0 and P_0 components, respectively (Mendel and Goldstein
664 1969; Picton et al. 1974; Yoshiura et al. 1996), indicating the transition between the ABR and
665 MLR. Of the four deflections observed, the P_0 was by far the weakest in terms of amplitude and
666 number of subjects with a significant response (i.e., 16 subjects; see **Table 1**).

667 Analysis of the MLR data (**Figure 3**) showed that at the group level, all MLR components
668 were evident (Na, Pa, Nb, Pb), along with ABR Wave V, which had a slightly later, broader peak
669 than in the ABR analysis. This shift in latency is likely due to the different bandpass filters
670 applied to the ABRs (100-1500 Hz) and MLRs (15-200 Hz), such that low-frequency activity
671 dominates the MLR representation of ABR Wave V. As shown in **Figure 3B**, the MLR
672 components peaked over frontal sites. At the single-subjects level in channel Fz, the majority of
673 participants had significant MLR components, but the Na and Pb were the most robust in terms
674 of amplitude and number of subjects with a significant response (22 and 20 subjects,
675 respectively). In channel Cz, there were 17, 15, 11, and 19 subjects showing significant Na, Pa,

676 Nb, and Pb responses, respectively. Furthermore, examination of the single-subject data in Fz
677 (p threshold of 0.001) revealed that all 25 subjects had at least one significant MLR component,
678 24 had at least two significant components, and 22 had at least three significant MLR
679 components.

680 The LLR data revealed a P1 that peaked at ~ 80 ms and was relatively broad in latency,
681 followed by an N1 that peaked at ~ 170 ms and a sustained negativity that was evident from
682 about 225 to 425 ms after voicing onsets in the Cheech (**Figure 4**). All three components had
683 fronto-central topography, suggestive of auditory cortex neural generators. Currently, it is
684 unclear if the observed sustained negativity reflects truly sustained activity and/or overlapping
685 N1's due to the continuous nature of the auditory stimulus. However, the topography of the
686 sustained negativity is very similar to the N1 topography. In channel Fz, all 25 subjects had a
687 significant P1, 21 had a significant N1, and 23 had a significant sustained negativity. In channel
688 Cz, the results were similar, but slightly weaker; 25, 19, and 22 subjects had a significant P1,
689 N1, and sustained negativity, respectively.

690 As illustrated in **Figure 5**, analysis of the VEP data revealed the visual P1, N1, and P2
691 components, followed by a late negativity over posterior sites, which started around 420 ms and
692 continued to the end of the epoch period. A subsequent examination of the group data, which
693 used a longer epoch (to 3 seconds beyond flicker onset), showed that this posterior negativity
694 continued until 770 ms after flicker onset. Inspection of the group-average scalp topographies
695 revealed that the visual P1 and N1 peaked over posterior sites, whereas the P2 showed a broad
696 scalp distribution that was maximal over midline sites across the scalp. At the single-subjects
697 level, a majority of participants had significant responses for each of the four components
698 identified. The P1 was the strongest in terms of number of subjects showing a significant
699 response (22 subjects), followed by the P2 and sustained negativity (20 subjects), and finally
700 the N1 (17 subjects). Furthermore, examination of the results in channel Oz (p -threshold of

701 0.001) revealed that all 25 subjects showed at least two VEP components significantly, and 19
702 had at least three components.

703 **Steady-State Responses (ASSR, SSVEP)**

704 **Table 2** contains a summary of the number of subjects showing a significant response
705 for each frequency of interest, along with the group raw magnitude and signal-to-noise ratio
706 (SNR) results.

707 Inspection of the ASSR data revealed large peaks at the stimulation frequency (41 Hz)
708 and its three harmonics (82 Hz, 123 Hz, 164 Hz), as displayed in **Figure 6**. At the group level,
709 the scalp location of maximum amplitude differed among the ASSR frequencies, with the lowest
710 frequency (41Hz) peaking fronto-centrally and the highest frequency (164Hz) peaking at the
711 vertex, possibly reflecting differential contributions from the ascending auditory pathway, in line
712 with Herdman et al. (2002) and Coffey et al. (2016). In the present study, the ASSR (and
713 SSVEP) raw magnitudes were first estimated by converting each epoch's time waveforms to the
714 frequency domain via a Fourier transform and then averaging across the frequency spectra,
715 within a bootstrapping algorithm. Similarly, the noise floor was modeled in similar fashion, with
716 the added step of randomizing phase (but preserving magnitude) before averaging frequency
717 spectra, as described in the Methods section. These raw magnitude and noise floor data were
718 used for statistical thresholding at the four frequencies of interest in channels Fz and Cz and
719 were used to compile the data in **Table 2**. All 25 subjects had significant ASSRs at 41, 123 and
720 164 Hz, and 24 of 25 subjects had significant responses at 82 Hz; this pattern of results was
721 observed in both Fz and Cz.

722 As shown in Figure 6B, the noise floor estimate accurately modeled the 1/f shape of the
723 noise floor in the actual ASSR data. However, the noise floor estimate was uniformly lower than
724 the raw magnitude estimate (red vs. blue line in Figure 6B), resulting in the floor of the signal-to-

725 noise ratio (SNR) hovering around 1.75 dB (black line) instead of 0 dB. This is suggestive of
726 broad-spectrum, weakly phase-locked neural activity that is driving the noise floor of the actual
727 ASSR data above what would be expected by chance (i.e., random phase across epochs). To
728 further probe this issue, we used a similar bootstrapping procedure to estimate the actual ASSR
729 data, but the epochs were averaged in time for each draw, and subsequently across 100 draws,
730 before converting it to frequency space. By averaging in time first, any weakly phase-locked
731 activity should be attenuated due to destructive interference. The resulting group average raw
732 magnitude spectrum is depicted in Figure 6B (gray line). Indeed, its noise floor is much lower
733 than both the noise floor estimate and original raw magnitude spectrum, while the peaks of both
734 raw magnitude spectra reached nearly identical values in channel Fz. This corroborates the
735 notion that weakly phase-locked activity contributes to the raw magnitude spectrum (and noise
736 floor estimation) averaged in the frequency domain.

737 Examination of the SSVEP data revealed peaks at the stimulation rates (7.5, 12 Hz) and
738 their first harmonics (15, 24 Hz), that were maximal over parieto-occipital sites (**Figure 7**). At
739 the individual subjects level, 21, 24, 22, and 19 subjects had significant neural responses at 7.5,
740 12, 15, and 24 Hz, respectively, in channel Oz as shown in **Table 2**. Furthermore, 20
741 participants had significant neural responses at both 7.5 and 12 Hz (stimulation fundamental
742 frequencies), and the other 5 subjects had significant responses at either 7.5 or 12 Hz.
743 However, like the ASSR, the noise floor estimate accurately reflected the $1/f$ shape of the noise
744 floor of the SSVEP magnitude spectrum, but it was uniformly ~ 1.2 dB lower than the apparent
745 noise floor in the actual SSVEP magnitude spectrum, obtained by averaging in frequency
746 space. Thus, we also computed SSVEP magnitude spectra, by averaging data in the time
747 domain first before converting to the frequency domain (Figure 7B, gray line). Like the ASSR,
748 the apparent noise floor of the time-averaged SSVEP spectrum dropped below that of the
749 estimated noise floor, again suggesting the contribution of weakly phase-locked neural activity

750 to the raw magnitude spectrum and noise floor estimation, which were averaged in the
751 frequency domain.

752 **Summary of ERP and Steady-State Response Results**

753 In summary, the paradigm was successful in eliciting multiple auditory and visual
754 responses across the subjects tested. For the ABR, LLR, ASSR, and SSVEP there was strong
755 convergence across subjects regarding which components were reliably detected. For the MLR
756 and VEP, the pattern was more heterogeneous; while nearly all subjects showed at least two or
757 three of the components within the MLR or VEP, these components were not necessarily the
758 same across participants. Nevertheless, these results demonstrate the robustness of our novel
759 paradigm.

760 **Assessing Relationships among Auditory and Visual EEG Responses**

761 We created individual aggregate z-scores for each of the auditory and visual responses,
762 by finding the z-score at the single-subject component peaks or for sustained responses,
763 averaging the z-scores across a pre-defined time range (i.e., 227-426 ms for LLR sustained
764 negativity; 422-496 for VEP late negativity). All ERP components described in the previous
765 section were included in these aggregate z-scores as follows: ABR: n_0 , Wave V, N_0 , P_0 ; MLR:
766 N_a , P_a , N_b , P_b ; LLR: P_1 , N_1 , sustained negativity; VEP: P_1 , N_1 , P_2 , late negativity. For the
767 ASSR and SSVEP, the individual z-scores were averaged across the four frequencies of
768 interest to create aggregate z-scores. All aggregate z-scores for each participant are shown in
769 **Figure 8**.

770 First, we conducted across-subjects pairwise Pearson correlations across the four
771 auditory responses (ABR, MLR, LLR, ASSR). Next, an across-subjects correlation was
772 computed between the VEP and SSVEP z-scores. Finally, we performed correlations within the
773 ASSR and SSVEP z-scores (all 25 subjects included), to determine if the magnitude at the

774 frequencies of interest were systematically related. None of the correlations were significant
775 after controlling for multiple comparisons, except for the correlation between the MLR and
776 ASSR ($r = 0.61$, $p = 0.001$, uncorrected) – which was likely driven by one participant. Therefore,
777 we did not observe any reliable systematic relationships among the different auditory and visual
778 EEG responses.

779 **Discussion**

780 We have developed a novel EEG paradigm to simultaneously record neural activity from
781 visual cortex, and from both subcortical and cortical auditory structures using a continuous
782 speech stimulus, in an unprecedentedly brief amount of time (6-12 min). To determine the
783 efficacy of this new paradigm, we have reported data from a group of healthy young adults.
784 Overall, most participants had significant responses for each of the components examined,
785 despite the conservative null distributions and the stringent p-value thresholds used for
786 statistical testing. The ABR, LLR, and ASSR tended to be the most robust responses, such that
787 all 25 participants had a significant response for the following components: ABR Wave V and
788 N₀, Auditory P1, and ASSR (41, 123, and 164 Hz). In terms of the number of participants who
789 showed significant responses, the SSVEP was next, followed by the VEP, and finally the MLR.
790 Furthermore, as described in the Results section, the pattern of results was most
791 heterogeneous for the VEP and MLR. While all 25 participants showed a significant response
792 for at least one MLR component and at least two VEP components, these were not always the
793 same MLR or VEP components across participants. This heterogeneous pattern partly reflects
794 our stringent statistical criteria and highlights the importance of examining the data, especially
795 the MLR and VEP, at the single-subjects level, particularly if this paradigm is used with clinical
796 populations. It also points to potential attributes of the audio and video stimuli that may be
797 further optimized to yield even more consistent responses across all subjects.

798 Based on an inspection of the ERP waveforms at the group level, the present paradigm
799 generally elicited the canonical responses, in terms of waveform morphology. The only
800 exceptions were the ABR, for which we did not observe the early waves before Wave V, and the
801 non-canonical LLR (which was expected). The ABR result is in contrast to a previous
802 implementation of the Cheech approach by our group, in which the early waves were observed,
803 using monaural delivery of the auditory stimuli via an insert earphone (Miller et al. 2017). Thus,
804 the lack of early waves in the present implementation may reflect the fact that the Cheech was
805 presented in the free-field. Furthermore, for the LLR, we observed the P1, N1, and a sustained
806 negativity, but not the P2 component, in response to voicing onsets within the continuous
807 Cheech. Notably, this morphology has been previously observed in studies using long-duration
808 sounds (Krishnan et al. 2012; Picton et al. 1978a; b), suggesting that this morphology is typical
809 when employing long-duration or continuous auditory stimuli. The present paradigm also
810 successfully evoked neural activity at the auditory stimulation rate (41 Hz) and its first three
811 harmonics (82, 123, and 164 Hz), in addition to neural activity at the visual stimulation rates (7.5
812 and 12 Hz) and their first harmonic (15 and 24 Hz). Taken together, these results demonstrate
813 that it is feasible to obtain all responses simultaneously, despite stimulating both auditory and
814 visual systems concurrently.

815 One advantage of obtaining a variety of responses simultaneously within individual
816 participants is that it allows for the assessment of relationships among the various responses.
817 Thus, in the present study, we conducted a series of correlations to understand if and how
818 different EEG responses' amplitude (converted to z-scores) related to one another. Overall, we
819 did not observe any robust across-subjects correlations among the different EEG responses.
820 This generally suggests that the examined responses reflect different processing operations
821 and/or different neural generators. Furthermore, assuming some inter-subject variability in EEG
822 recording quality, the lack of uniform relationships across responses indicates that recording

823 quality variability is unlikely to induce false across-subjects correlations among the different
824 EEG responses. Moreover, by examining all responses simultaneously, the lack of systematic
825 relationships among the EEG responses within subjects cannot be due to changes in for
826 example, brain state or alertness, across time, as is the case for serial recording paradigms.
827 Taken together, these points highlight the importance of assessing all responses simultaneously
828 for a thorough evaluation of the auditory and visual systems – which the current EEG paradigm
829 enables.

830 Previously, a variety of paradigms have been developed to record EEG activity at
831 multiple processing levels, using auditory stimuli. Here, we compare these previous paradigms
832 to the current one, in terms of the responses recorded, whether the different responses were
833 recorded simultaneously or serially, the type of stimuli used, and the EEG recording duration.

834 First, regarding the responses recorded, previous paradigms have mostly recorded the
835 subcortical (usually frequency-following response (FFR)) and cortical (i.e., LLR) activity
836 (Bidelman 2015; Bidelman and Alain 2015; Bidelman et al. 2013; Bidelman et al. 2014a;
837 Bidelman et al. 2014b; Krishnan et al. 2012; Musacchia et al. 2008). Woods et al. (1993)
838 analyzed the ABR, MLR, and LLR; similarly, Shiga et al. (2015) developed a paradigm to
839 examine the FFR, MLR, and LLR (MMN). Slugocki and colleagues (2017) measured a variety
840 of subcortical and cortical responses, including FFR, 40- and 80-Hz ASSR, LLR, MMN, and
841 P3a. Finally, Sculthorpe-Petley et al.'s (2015) paradigm measured only cortical responses,
842 including LLR (N1), MMN, P300, N400, and Early Negative Enhancement (reflects recognition
843 of hearing one own's name; Holler et al. 2011; Tateuchi et al. 2012). In contrast, the present
844 paradigm enables the recording of subcortical and cortical auditory activity (ABR, MLR, LLR,
845 ASSR), as well as cortical visual activity (VEP, SSVEP).

846 With respect to how both auditory subcortical and cortical responses were recorded,
847 various approaches have been used. Subcortical responses occur earlier and thus necessitate
848 smaller inter-stimulus intervals (ISIs) and higher EEG acquisition sampling rates than cortical
849 responses. Many studies have recorded brainstem and cortical responses sequentially in
850 separate blocks (e.g., Bidelman and Alain 2015; Bidelman et al. 2013; Bidelman et al. 2014a;
851 Bidelman et al. 2014b; Musacchia et al. 2008) or in interleaved clusters (Bidelman 2015); these
852 approaches usually involve using shorter ISIs for the brainstem blocks/clusters than the cortical
853 blocks/clusters. Other studies have recorded auditory brainstem and cortical responses
854 simultaneously, using fixed ISIs (e.g., Krishnan et al. 2012; Shiga et al. 2015; Slugocki et al.
855 2017) or variable ISIs (e.g., 40 to 200 ms; Woods et al. 1993) to accommodate both types of
856 responses.

857 Regarding the types of auditory stimuli used, previous studies have employed amplitude-
858 modulated tones (Shiga et al. 2015; Slugocki et al. 2017), tone pips in the midst of broadband
859 masking noise (Woods et al. 1993), iterated rippled noise stimuli (Krishnan et al. 2012), and
860 synthetic vowel or consonant-vowel stimuli (e.g., Bidelman 2015; Bidelman et al. 2013;
861 Musacchia et al. 2008). Sculthorpe-Petley and colleagues' (2015) paradigm used tones in one
862 half of the recording, and continuous speech (sentences) in the other half. In the present study,
863 the use of chirps embedded into continuous speech (Cheech) allows for the simultaneous
864 recording of subcortical and cortical activity in response to a naturalistic stimulus.

865 With respect to EEG recording duration, the fastest of these studies was that by Petley-
866 Sculthorpe et al. (2015), which approximated only 5 minutes; however, only cortical responses
867 were recorded. For paradigms involving recording both subcortical and cortical responses,
868 Bidelman's (2015) clustering approach took approximately 28 minutes, while the paradigm
869 described in Shiga et al. (2015) lasted around 38 minutes. Likewise, Slugocki and colleagues'
870 (2017) paradigm involved about 40 minutes of recording time. In contrast, the paradigm

871 described herein involves 12 minutes maximum of recording time – which is considerably faster
872 than these other approaches devised to collect both subcortical and cortical auditory responses.

873 In fact, the present data were collected in only 12 minutes, mainly to allow for enough
874 trials for the originally planned black-white versus red-green comparison (6 minutes per color
875 condition). We have used a 10-minute black-white-only version of this paradigm to collect data
876 in young children, which is ample time to yield reliable ERPs for most children, even after noisy
877 data segments and epochs were removed (unpublished data from our laboratory). The brief
878 time required makes this paradigm ideal for individuals who are unable to sit through a long
879 study (e.g., toddlers), and allows for short study sessions, which is advantageous to both busy
880 participants and researchers.

881 Furthermore, in the present EEG paradigm, participants watched cartoon clips during the
882 presentation of the visual flicker and auditory Cheech stimuli. This was done to render the
883 paradigm infant/child friendly. Also, because this task requires no behavioral responses, it can
884 be used in infants and young children, as well as in individuals with limited communication
885 abilities. That said, the paradigm can also easily be adapted into an active task, for instance to
886 investigate top-down attention effects on the various auditory and visual responses recorded.

887 Along these lines, one caveat of the present implementation is that although participants
888 were instructed to watch the cartoon clips, they were not explicitly told to ignore the flicker or
889 Cheech stimuli. Thus, it is important to acknowledge that participants' attention likely wandered
890 to the flicker or Cheech stimuli at times, and consequently, it is important to acknowledge the
891 known effects of attention on the measured responses. Selective attention to or away from a
892 particular auditory stimulus has been shown to have little to no effect on the ABR (Hackley et al.
893 1990; Woldorff and Hillyard 1991), a small effect on the MLR, particularly after 20 ms (Hackley
894 et al. 1990; Woldorff et al. 1987), and the most robust effect on the LLR, particularly the N1 and

895 P2 components (Hillyard et al. 1973; Picton et al. 1971). Similarly, attending (or not) to a visual
896 stimulus affects the VEP, especially from the P1 and later (e.g., Clark and Hillyard 1996; Gomez
897 Gonzalez et al. 1994; Mangun et al. 1993). Furthermore, there is evidence that selective
898 attention can enhance the 40-Hz ASSR to the attended sound's stimulation rate (Bharadwaj et
899 al. 2014; Tiitinen et al. 1993) (but see Mahajan et al. 2014; Muller et al. 2009) and the SSVEP to
900 the attended visual stimulus' stimulation rate (Andersen et al. 2015; Morgan et al. 1996). Thus,
901 these findings indicate that selective attention has a stronger effect on the neural response to a
902 stimulus as it ascends from sub-cortical to cortical processing regions.

903 Since attention was not explicitly manipulated in the current paradigm, future studies can
904 use this paradigm in conjunction with an attention manipulation, to quantify how selective
905 attention modulates the recorded responses. Furthermore, in the present study, participants
906 watched a cartoon while also perceiving flickering visual stimuli. Thus, it is possible that if
907 participants generally devoted more visual attention to the cartoon than the visual flickers, then
908 they would elicit smaller VEPs and SSVEPs than if these stimuli had been actively attended.
909 This explanation may account for the fact that the VEP and SSVEP measures were significantly
910 detected in fewer subjects overall than the ABR, LLR, and ASSR. Despite this caveat, we
911 observed the VEP components and SSVEP responses in a majority of participants; this
912 suggests that even if reduced attention to the flickers has an effect on the visual responses, it
913 does not eradicate them in the present paradigm.

914 Furthermore, this paradigm is flexible, in that the visual and auditory stimuli can be
915 customized according to one's particular research questions. For example, including audio-only
916 and visual-only periods of stimulation, along with concurrent auditory and visual stimulation, one
917 could directly examine how activity may be modulated by the stimulus context in an individual.
918 Moreover, the concurrent auditory and visual stimuli also present opportunities for the
919 examination of complex interactions between the auditory and visual systems. For example,

920 this use of multisensory stimulation may provide new and important data on one's ability to deal
921 with multiple and competing sensory information. However, the multisensory nature of this
922 paradigm is not limited to competing or distracting visual stimuli. Alternatively, future
923 implementations of this paradigm could use congruent and incongruent talking face stimuli that
924 coincide with the Cheech, to study neural mechanisms involved in audiovisual integration of
925 speech. Regarding feasibility in terms of accurate EEG trigger timing, careful attention to timing
926 is important when implementing the current EEG paradigm. First, when implementing the
927 present paradigm, it is important to quantify timing differences between the trigger codes and
928 stimuli and to determine if any auditory trigger codes are being missed, using an oscilloscope.
929 Next, if timing inconsistencies are observed, there are various ways to address this. One way
930 would be to adjust triggers and add missing triggers post-hoc, using the approach that we have
931 developed; our MATLAB code for this approach has been posted on GitHub at
932 <https://github.com/MillerLab-UCDavis/Cheech-Toolbox>. There are also other ways to obtain
933 accurate trigger timing; for example, one could play a third audio channel that contains only
934 trigger pulses and send that signal to the EEG system directly, or one could use a third-party
935 device designed for accurate trigger timing, such as the Cedrus StimTracker. Therefore,
936 obtaining precise trigger timing when implementing the present EEG paradigm is feasible.

937 There are various potential applications of this paradigm to clinical research, even
938 beyond assessing auditory function in the context of hearing loss. For example, its utility may be
939 investigated in patients with multiple sclerosis (MS), as previous studies have indicated
940 usefulness of auditory evoked potentials (especially ABRs and MLRs) for detecting neurological
941 abnormalities in some cases (e.g., Celebisoy et al. 1996; Japaridze et al. 2002; Soustiel et al.
942 1996). Moreover, this paradigm would additionally allow for the assessment of visual cortical
943 responses in these patients, especially since visual disturbances are one of the most common
944 reported signs in patients with MS (Milner et al. 1974). In another context, the multisensory

945 nature of the paradigm can be harnessed to investigate interactions between auditory and visual
946 processing in children with hearing loss (Backer et al. 2017) or in children with autism spectrum
947 disorder or auditory and language processing disorders. These are just a few examples of
948 many potential applications.

949 Future research involving this paradigm, especially that involving clinical populations, will
950 provide valuable information regarding the generalizability of the present results. We should
951 make clear that the technique is free and unrestricted for non-commercial research and
952 educational use, in accordance with the University of California's "Principles Regarding Rights
953 to Future Research Results" guidelines (see Principle #3 at [https://www.ucop.edu/research-
954 policy-analysis-coordination/ files/Principles%20Guidelines.pdf](https://www.ucop.edu/research-policy-analysis-coordination/files/Principles%20Guidelines.pdf)). For more information or to
955 inquire about a license for commercial use or commercial applications, please contact the UC
956 Davis Office of Research at innovationAccess@ucdavis.edu.

957 In conclusion, we have demonstrated the use of a new EEG paradigm to concurrently
958 stimulate and record subcortical and cortical auditory activity, as well as parafoveal and
959 peripheral cortical visual activity, in about 6-12 minutes. In light of the short recording time and
960 the flexibility to customize the auditory and visual stimuli depending on the study's population
961 and goals, this EEG paradigm may be useful for both basic and clinical research objectives.

962

963

964

965

966

967 **Acknowledgements**

968 The authors are grateful to Todd LaMarr, Ludmila Ciochina, Surah Alsawaf, Danielle Fujino, and
969 Alaina Porter for their assistance with data collection. Thanks to the House Ear Institute for
970 providing the Harvard/IEEE recordings.

971 Please note Laurel A. Lawyer's present affiliation: Department of Language and Linguistics,
972 University of Essex, Colchester, UK. Andrew S. Kessler's present affiliation: Verathon Inc.,
973 Division of Imaging and Scanning Solutions, Bothell, WA.

974

975 **Grants**

976 Funding from the National Institutes of Health, National Institute on Deafness and Other
977 Communication Disorders (Grant DC014767 awarded to DPC), the Child Family Fund for the
978 Center for Mind and Brain (awarded to LMM and DPC), and the UC Davis Science Translation
979 and Innovative Research (STAIR) grant (awarded to LMM) supported this research.

980

981 **Disclosures**

982 As noted in the manuscript, the chirp-speech approach is patent-pending and owned by the
983 Regents of the University of California, with Lee M. Miller as inventor. The University of
984 California encourages the use of this technique for non-commercial educational and research
985 purposes. For more information or to inquire about a license for commercial use or commercial
986 applications, please contact the UC Davis Office of Research at
987 innovationAccess@ucdavis.edu. No financial or other conflicts of interest (e.g., licensing
988 agreements) exist.

989 **Footnotes**

990 ¹ In many reports, the terms “Pb” (MLR component) and “P1” (LLR component) are used
991 interchangeably, due to overlapping time courses. However, the Pb and P1 may have different
992 neural generators and developmental trajectories (Ponton et al. 2002), suggesting that they may
993 index different aspects of auditory processing.

994 ² Acoustic periodicity can also elicit another type of auditory response, the frequency following
995 response (FFR) (for reviews, see Krishnan 2007; Skoe and Kraus 2010), which is traditionally
996 thought to have neural generators in sub-cortical structures (Chandrasekaran and Kraus 2010),
997 but recent studies suggest additional contributions from the auditory cortex (Coffey et al. 2016),
998 if stimulus frequency is relatively low (Bidelman 2018). However, further discussion of the FFR
999 is beyond the scope of the present report.

1000

1001

1002

1003

1004

1005

1006

1007

1008

1009

- 1011 IEEE Recommended Practice for Speech Quality Measurements. *IEEE No 297-1969* 1-24,
1012 1969.
- 1013 **Aine CJ, Supek S, and George JS.** Temporal dynamics of visual-evoked neuromagnetic
1014 sources: effects of stimulus parameters and selective attention. *Int J Neurosci* 80: 79-104, 1995.
- 1015 **Andersen SK, Hillyard SA, and Muller MM.** Attention facilitates multiple stimulus features in
1016 parallel in human visual cortex. *Curr Biol* 18: 1006-1009, 2008.
- 1017 **Andersen SK, Muller MM, and Hillyard SA.** Attentional Selection of Feature Conjunctions Is
1018 Accomplished by Parallel and Independent Selection of Single Features. *J Neurosci* 35: 9912-
1019 9919, 2015.
- 1020 **Arslan E, Prosser S, and Michelini S.** Simultaneous recording of auditory evoked potentials.
1021 Relationships among the fast, middle and long latency components. *Scand Audiol* 13: 75-81,
1022 1984.
- 1023 **Artieda J, Valencia M, Alegre M, Olaziregi O, Urrestarazu E, and Iriarte J.** Potentials evoked
1024 by chirp-modulated tones: a new technique to evaluate oscillatory activity in the auditory
1025 pathway. *Clin Neurophysiol* 115: 699-709, 2004.
- 1026 **Backer KC, Kessler AS, Coffey-Corina S, Lawyer LA, Miller LM, and Corina DP.** Abstract:
1027 Charting developmental changes in auditory and visual evoked potentials in children with
1028 cochlear implants. In: *Conference on Implantable Auditory Protheses*. Lake Tahoe, CA: 2017.
- 1029 **Bell AJ, and Sejnowski TJ.** An information-maximization approach to blind separation and
1030 blind deconvolution. *Neural Comput* 7: 1129-1159, 1995.
- 1031 **Bell SL, Allen R, and Lutman ME.** An investigation of the use of band-limited chirp stimuli to
1032 obtain the auditory brainstem response. *Int J Audiol* 41: 271-278, 2002a.
- 1033 **Bell SL, Allen R, and Lutman ME.** Optimizing the acquisition time of the middle latency
1034 response using maximum length sequences and chirps. *J Acoust Soc Am* 112: 2065-2073,
1035 2002b.
- 1036 **Bharadwaj HM, Lee AK, and Shinn-Cunningham BG.** Measuring auditory selective attention
1037 using frequency tagging. *Front Integr Neurosci* 8: 6, 2014.
- 1038 **Bidelman GM.** Subcortical sources dominate the neuroelectric auditory frequency-following
1039 response to speech. *Neuroimage* 175: 56-69, 2018.
- 1040 **Bidelman GM.** Towards an optimal paradigm for simultaneously recording cortical and
1041 brainstem auditory evoked potentials. *J Neurosci Methods* 241: 94-100, 2015.
- 1042 **Bidelman GM, and Alain C.** Musical training orchestrates coordinated neuroplasticity in
1043 auditory brainstem and cortex to counteract age-related declines in categorical vowel
1044 perception. *J Neurosci* 35: 1240-1249, 2015.
- 1045 **Bidelman GM, Moreno S, and Alain C.** Tracing the emergence of categorical speech
1046 perception in the human auditory system. *Neuroimage* 79: 201-212, 2013.
- 1047 **Bidelman GM, Villafuerte JW, Moreno S, and Alain C.** Age-related changes in the
1048 subcortical-cortical encoding and categorical perception of speech. *Neurobiol Aging* 35: 2526-
1049 2540, 2014a.
- 1050 **Bidelman GM, Weiss MW, Moreno S, and Alain C.** Coordinated plasticity in brainstem and
1051 auditory cortex contributes to enhanced categorical speech perception in musicians. *Eur J*
1052 *Neurosci* 40: 2662-2673, 2014b.
- 1053 **Boersma P, and Weenink D.** *PRAAT, a system for doing phonetics by computer*. 2001, p. 341-
1054 345.
- 1055 **Burkitt GR, Silberstein RB, Cadusch PJ, and Wood AW.** Steady-state visual evoked
1056 potentials and travelling waves. *Clin Neurophysiol* 111: 246-258, 2000.
- 1057 **Celebisoy N, Aydogdu I, Ekmekci O, and Akurekli O.** Middle latency auditory evoked
1058 potentials (MLAEPs) in (MS). *Acta Neurol Scand* 93: 318-321, 1996.

1059 **Celesia GG**. Organization of auditory cortical areas in man. *Brain* 99: 403-414, 1976.

1060 **Chandrasekaran B, and Kraus N**. The scalp-recorded brainstem response to speech: neural
1061 origins and plasticity. *Psychophysiology* 47: 236-246, 2010.

1062 **Clark VP, Fan S, and Hillyard SA**. Identification of early visual evoked potential generators by
1063 retinotopic and topographic analyses. *Human Brain Mapping* 2: 170-187, 1994.

1064 **Clark VP, and Hillyard SA**. Spatial selective attention affects early extrastriate but not striate
1065 components of the visual evoked potential. *J Cogn Neurosci* 8: 387-402, 1996.

1066 **Coffey EB, Herholz SC, Chepesiuk AM, Baillet S, and Zatorre RJ**. Cortical contributions to
1067 the auditory frequency-following response revealed by MEG. *Nat Commun* 7: 11070, 2016.

1068 **Cowey A, and Rolls ET**. Human cortical magnification factor and its relation to visual acuity.
1069 *Exp Brain Res* 21: 447-454, 1974.

1070 **Daniel PM, and Whitteridge D**. The representation of the visual field on the cerebral cortex in
1071 monkeys. *J Physiol* 159: 203-221, 1961.

1072 **Dau T, Wegner O, Mellert V, and Kollmeier B**. Auditory brainstem responses with optimized
1073 chirp signals compensating basilar-membrane dispersion. *J Acoust Soc Am* 107: 1530-1540,
1074 2000.

1075 **Davis H, and Zerlin S**. Acoustic relations of the human vertex potential. *J Acoust Soc Am* 39:
1076 109-116, 1966.

1077 **Davis PA**. Effects of acoustic stimuli on the waking human brain. *Journal of Neurophysiology* 2:
1078 494-499, 1939.

1079 **Delorme A, and Makeig S**. EEGLAB: an open source toolbox for analysis of single-trial EEG
1080 dynamics including independent component analysis. *J Neurosci Methods* 134: 9-21, 2004.

1081 **Di Russo F, Martinez A, Sereno MI, Pitzalis S, and Hillyard SA**. Cortical sources of the early
1082 components of the visual evoked potential. *Hum Brain Mapp* 15: 95-111, 2002.

1083 **Di Russo F, Pitzalis S, Spitoni G, Aprile T, Patria F, Spinelli D, and Hillyard SA**.
1084 Identification of the neural sources of the pattern-reversal VEP. *Neuroimage* 24: 874-886, 2005.

1085 **Ding J, Sperling G, and Srinivasan R**. Attentional modulation of SSVEP power depends on
1086 the network tagged by the flicker frequency. *Cereb Cortex* 16: 1016-1029, 2006.

1087 **Elberling C, and Don M**. Auditory brainstem responses to a chirp stimulus designed from
1088 derived-band latencies in normal-hearing subjects. *J Acoust Soc Am* 124: 3022-3037, 2008.

1089 **Elberling C, Don M, Cebulla M, and Sturzebecher E**. Auditory steady-state responses to chirp
1090 stimuli based on cochlear traveling wave delay. *J Acoust Soc Am* 122: 2772-2785, 2007.

1091 **Galambos R, Makeig S, and Talmachoff PJ**. A 40-Hz auditory potential recorded from the
1092 human scalp. *Proc Natl Acad Sci U S A* 78: 2643-2647, 1981.

1093 **Geisler CD, Frishkopf LS, and Rosenblith WA**. Extracranial responses to acoustic clicks in
1094 man. *Science* 128: 1210-1211, 1958.

1095 **Goldstein R, and Rodman LB**. Early components of averaged evoked responses to rapidly
1096 repeated auditory stimuli. *J Speech Hear Res* 10: 697-705, 1967.

1097 **Gomez Gonzalez CM, Clark VP, Fan S, Luck SJ, and Hillyard SA**. Sources of attention-
1098 sensitive visual event-related potentials. *Brain Topogr* 7: 41-51, 1994.

1099 **Hackley SA, Woldorff M, and Hillyard SA**. Cross-modal selective attention effects on retinal,
1100 myogenic, brainstem, and cerebral evoked potentials. *Psychophysiology* 27: 195-208, 1990.

1101 **Halgren E**. Human Evoked Potentials. In: *Neurophysiological Techniques: Applications to*
1102 *Neural Systems*, edited by Boulton AA, Baker GB, and Vanderwolf CH. Totowa, NJ: Humana
1103 Press, 1990, p. 147-275.

1104 **Hall JW**. *New Handbook of Auditory Evoked Responses*. Pearson, 2007.

1105 **Hari R, Aittoniemi K, Jarvinen ML, Katila T, and Varpula T**. Auditory evoked transient and
1106 sustained magnetic fields of the human brain. Localization of neural generators. *Exp Brain Res*
1107 40: 237-240, 1980.

1108 **Hashimoto I**. Auditory evoked potentials from the human midbrain: slow brain stem responses.
1109 *Electroencephalogr Clin Neurophysiol* 53: 652-657, 1982.

1110 **Hashimoto I, Ishiyama Y, and Tozuka G.** Bilaterally recorded brain stem auditory evoked
1111 responses. Their asymmetric abnormalities and lesions of the brain stem. *Arch Neurol* 36: 161-
1112 167, 1979.

1113 **Herdman AT, Lins O, Van Roon P, Stapells DR, Scherg M, and Picton TW.** Intracerebral
1114 sources of human auditory steady-state responses. *Brain Topogr* 15: 69-86, 2002.

1115 **Hillyard SA, Hink RF, Schwent VL, and Picton TW.** Electrical signs of selective attention in
1116 the human brain. *Science* 182: 177-180, 1973.

1117 **Holler Y, Kronbichler M, Bergmann J, Crone JS, Ladurner G, and Golaszewski S.** EEG
1118 frequency analysis of responses to the own-name stimulus. *Clin Neurophysiol* 122: 99-106,
1119 2011.

1120 **Itthipuripat S, Garcia JO, and Serences JT.** Temporal dynamics of divided spatial attention. *J*
1121 *Neurophysiol* 109: 2364-2373, 2013.

1122 **Japaridze G, Shakarishvili R, and Kevanishvili Z.** Auditory brainstem, middle-latency, and
1123 slow cortical responses in multiple sclerosis. *Acta Neurol Scand* 106: 47-53, 2002.

1124 **Jeffreys DA, and Axford JG.** Source locations of pattern-specific components of human visual
1125 evoked potentials. I. Component of striate cortical origin. *Exp Brain Res* 16: 1-21, 1972.

1126 **Jewett DL, and Williston JS.** Auditory-evoked far fields averaged from the scalp of humans.
1127 *Brain* 94: 681-696, 1971.

1128 **Kanno A, Nakasato N, Murayama N, and Yoshimoto T.** Middle and long latency peak
1129 sources in auditory evoked magnetic fields for tone bursts in humans. *Neurosci Lett* 293: 187-
1130 190, 2000.

1131 **Keitel C, Andersen SK, and Muller MM.** Competitive effects on steady-state visual evoked
1132 potentials with frequencies in- and outside the alpha band. *Exp Brain Res* 205: 489-495, 2010.

1133 **Kileny P, Paccioretti D, and Wilson AF.** Effects of cortical lesions on middle-latency auditory
1134 evoked responses (MLR). *Electroencephalogr Clin Neurophysiol* 66: 108-120, 1987.

1135 **Korczak P, Smart J, Delgado R, Strobel TM, and Bradford C.** Auditory steady-state
1136 responses. *J Am Acad Audiol* 23: 146-170, 2012.

1137 **Kraus N, McGee T, Carrell T, Sharma A, Micco A, and Nicol T.** Speech-evoked cortical
1138 potentials in children. *J Am Acad Audiol* 4: 238-248, 1993.

1139 **Kraus N, Ozdamar O, Hier D, and Stein L.** Auditory middle latency responses (MLRs) in
1140 patients with cortical lesions. *Electroencephalogr Clin Neurophysiol* 54: 275-287, 1982.

1141 **Krishnan A.** Human frequency following response. In: *Auditory evoked potentials: basic*
1142 *principles and clinical application*, edited by Burkard RF, Don JJ, and Eggermont JJ. Baltimore:
1143 Lippincott Williams & Wilkins, 2007, p. 315-335.

1144 **Krishnan A, Bidelman GM, Smalt CJ, Ananthkrishnan S, and Gandour JT.** Relationship
1145 between brainstem, cortical and behavioral measures relevant to pitch salience in humans.
1146 *Neuropsychologia* 50: 2849-2859, 2012.

1147 **Krizman JL, Skoe E, and Kraus N.** Stimulus rate and subcortical auditory processing of
1148 speech. *Audiol Neurootol* 15: 332-342, 2010.

1149 **Lee YS, Lueders H, Dinner DS, Lesser RP, Hahn J, and Klem G.** Recording of auditory
1150 evoked potentials in man using chronic subdural electrodes. *Brain* 107 (Pt 1): 115-131, 1984.

1151 **Liegeois-Chauvel C, Musolino A, Badier JM, Marquis P, and Chauvel P.** Evoked potentials
1152 recorded from the auditory cortex in man: evaluation and topography of the middle latency
1153 components. *Electroencephalogr Clin Neurophysiol* 92: 204-214, 1994.

1154 **Lopez-Calderon J, and Luck SJ.** ERPLAB: an open-source toolbox for the analysis of event-
1155 related potentials. *Front Hum Neurosci* 8: 213, 2014.

1156 **Luck SJ.** *An Introduction to the Event-Related Potential Technique.* Cambridge,
1157 Massachusetts; London, England: The MIT Press, 2014.

1158 **Luck SJ, Kappenman ES. (Eds.)** *Oxford Library of Psychology. The Oxford Handbook of*
1159 *Event-Related Potential Components.* New York, NY: Oxford University Press, 2011.

1160 **Mahajan Y, Davis C, and Kim J.** Attentional modulation of auditory steady-state responses.
1161 *PLoS One* 9: e110902, 2014.

1162 **Makela JP, and Hari R.** Evidence for cortical origin of the 40 Hz auditory evoked response in
1163 man. *Electroencephalogr Clin Neurophysiol* 66: 539-546, 1987.

1164 **Mangun GR, Hillyard SA, and Luck SJ.** Electro cortical substrates of visual selective attention.
1165 In: *Attention and performance XIV (silver jubilee volume)*, edited by David EM, and Sylvan KMIT
1166 Press, 1993, p. 219-243.

1167 **Mendel MI, and Goldstein R.** Stability of the early components of the averaged
1168 electroencephalic response. *J Speech Hear Res* 12: 351-361, 1969.

1169 **Miller L, Moore IVB, and Bishop C.** (Patent Pending). Frequency-multiplexed speech-sound
1170 stimuli for hierarchical neural characterization of speech processing. United States: The
1171 Regents of the University of California, 2017.
1172 <https://patents.google.com/patent/US20170196519A1/en>

1173 **Milner BA, Regan D, and Heron JR.** Differential diagnosis of multiple sclerosis by visual
1174 evoked potential recording. *Brain* 97: 755-772, 1974.

1175 **Moller AR, Jannetta P, and Moller MB.** Intracranially recorded auditory nerve response in
1176 man. New interpretations of BSER. *Arch Otolaryngol* 108: 77-82, 1982.

1177 **Moller AR, Jannetta PJ, and Moller MB.** Neural generators of brainstem evoked potentials.
1178 Results from human intracranial recordings. *Ann Otol Rhinol Laryngol* 90: 591-596, 1981.

1179 **Moore JK.** The human auditory brain stem as a generator of auditory evoked potentials. *Hear*
1180 *Res* 29: 33-43, 1987.

1181 **Morgan ST, Hansen JC, and Hillyard SA.** Selective attention to stimulus location modulates
1182 the steady-state visual evoked potential. *Proc Natl Acad Sci U S A* 93: 4770-4774, 1996.

1183 **Muller MM, Malinowski P, Gruber T, and Hillyard SA.** Sustained division of the attentional
1184 spotlight. *Nature* 424: 309-312, 2003.

1185 **Muller N, Schlee W, Hartmann T, Lorenz I, and Weisz N.** Top-down modulation of the
1186 auditory steady-state response in a task-switch paradigm. *Front Hum Neurosci* 3: 1, 2009.

1187 **Musacchia G, Strait D, and Kraus N.** Relationships between behavior, brainstem and cortical
1188 encoding of seen and heard speech in musicians and non-musicians. *Hear Res* 241: 34-42,
1189 2008.

1190 **Naatanen R, and Picton T.** The N1 wave of the human electric and magnetic response to
1191 sound: a review and an analysis of the component structure. *Psychophysiology* 24: 375-425,
1192 1987.

1193 **Norcia AM, Appelbaum LG, Ales JM, Cottureau BR, and Rossion B.** The steady-state visual
1194 evoked potential in vision research: A review. *J Vis* 15: 4, 2015.

1195 **Pelizzone M, Hari R, Makela JP, Huttunen J, Ahlfors S, and Hamalainen M.** Cortical origin of
1196 middle-latency auditory evoked responses in man. *Neurosci Lett* 82: 303-307, 1987.

1197 **Perrault N, and Picton TW.** Event-related potentials recorded from the scalp and nasopharynx.
1198 I. N1 and P2. *Electroencephalogr Clin Neurophysiol* 59: 177-194, 1984.

1199 **Picton TW, Alain C, Woods DL, John MS, Scherg M, Valdes-Sosa P, Bosch-Bayard J, and**
1200 **Trujillo NJ.** Intracerebral sources of human auditory-evoked potentials. *Audiol Neurootol* 4: 64-
1201 79, 1999.

1202 **Picton TW, Hillyard SA, Galambos R, and Schiff M.** Human auditory attention: a central or
1203 peripheral process? *Science* 173: 351-353, 1971.

1204 **Picton TW, Hillyard SA, Krausz HI, and Galambos R.** Human auditory evoked potentials. I.
1205 Evaluation of components. *Electroencephalogr Clin Neurophysiol* 36: 179-190, 1974.

1206 **Picton TW, John MS, Dimitrijevic A, and Purcell D.** Human auditory steady-state responses.
1207 *Int J Audiol* 42: 177-219, 2003.

1208 **Picton TW, Woods DL, and Proulx GB.** Human auditory sustained potentials. I. The nature of
1209 the response. *Electroencephalogr Clin Neurophysiol* 45: 186-197, 1978a.

1210 **Picton TW, Woods DL, and Proulx GB.** Human auditory sustained potentials. II. Stimulus
1211 relationships. *Electroencephalogr Clin Neurophysiol* 45: 198-210, 1978b.

1212 **Ponton C, Eggermont JJ, Khosla D, Kwong B, and Don M.** Maturation of human central
1213 auditory system activity: separating auditory evoked potentials by dipole source modeling. *Clin*
1214 *Neurophysiol* 113: 407-420, 2002.

1215 **Pratt H, and Sohmer H.** Intensity and rate functions of cochlear and brainstem evoked
1216 responses to click stimuli in man. *Arch Otorhinolaryngol* 212: 85-92, 1976.

1217 **Regan D.** Some characteristics of average steady-state and transient responses evoked by
1218 modulated light. *Electroencephalography and Clinical Neurophysiology* 20: 238-248, 1966.

1219 **Regan D.** Steady-state evoked potentials. *J Opt Soc Am* 67: 1475-1489, 1977.

1220 **Regan D, and Heron JR.** Clinical investigation of lesions of the visual pathway: a new objective
1221 technique. *J Neurol Neurosurg Psychiatry* 32: 479-483, 1969.

1222 **Ross B, Picton TW, and Pantev C.** Temporal integration in the human auditory cortex as
1223 represented by the development of the steady-state magnetic field. *Hear Res* 165: 68-84, 2002.

1224 **Rupp A, Uppenkamp S, Gutschalk A, Beucker R, Patterson RD, Dau T, and Scherg M.** The
1225 representation of peripheral neural activity in the middle-latency evoked field of primary auditory
1226 cortex in humans(1). *Hear Res* 174: 19-31, 2002.

1227 **Scherg M, and Von Cramon D.** Evoked dipole source potentials of the human auditory cortex.
1228 *Electroencephalogr Clin Neurophysiol* 65: 344-360, 1986.

1229 **Scherg M, and Von Cramon D.** Two bilateral sources of the late AEP as identified by a spatio-
1230 temporal dipole model. *Electroencephalogr Clin Neurophysiol* 62: 32-44, 1985.

1231 **Schoonhoven R, Boden CJ, Verbunt JP, and de Munck JC.** A whole head MEG study of the
1232 amplitude-modulation-following response: phase coherence, group delay and dipole source
1233 analysis. *Clin Neurophysiol* 114: 2096-2106, 2003.

1234 **Sculthorpe-Petley L, Liu C, Hajra SG, Parvar H, Satel J, Trappenberg TP, Boshra R, and**
1235 **D'Arcy RC.** A rapid event-related potential (ERP) method for point-of-care evaluation of brain
1236 function: development of the Halifax Consciousness Scanner. *J Neurosci Methods* 245: 64-72,
1237 2015.

1238 **Shahin AJ, Roberts LE, Miller LM, McDonald KL, and Alain C.** Sensitivity of EEG and MEG
1239 to the N1 and P2 auditory evoked responses modulated by spectral complexity of sounds. *Brain*
1240 *Topogr* 20: 55-61, 2007.

1241 **Shiga T, Althen H, Cornella M, Zarnowiec K, Yabe H, and Escera C.** Deviance-Related
1242 Responses along the Auditory Hierarchy: Combined FFR, MLR and MMN Evidence. *PLoS One*
1243 10: e0136794, 2015.

1244 **Shore SE, and Nuttall AL.** High-synchrony cochlear compound action potentials evoked by
1245 rising frequency-swept tone bursts. *J Acoust Soc Am* 78: 1286-1295, 1985.

1246 **Skoe E, and Kraus N.** Auditory brain stem response to complex sounds: a tutorial. *Ear Hear*
1247 31: 302-324, 2010.

1248 **Slugocki C, Bosnyak D, and Trainor LJ.** Simultaneously-evoked auditory potentials (SEAP): A
1249 new method for concurrent measurement of cortical and subcortical auditory-evoked activity.
1250 *Hear Res* 345: 30-42, 2017.

1251 **Soustiel JF, Hafner H, Chistyakov AV, Yarnitzky D, Sharf B, Guilburd JN, and Feinsod M.**
1252 Brain-stem trigeminal and auditory evoked potentials in multiple sclerosis: physiological insights.
1253 *Electroencephalogr Clin Neurophysiol* 100: 152-157, 1996.

1254 **Stapells DR, Linden D, Suffield JB, Hamel G, and Picton TW.** Human auditory steady state
1255 potentials. *Ear Hear* 5: 105-113, 1984.

1256 **Starr A, and Hamilton AE.** Correlation between confirmed sites of neurological lesions and
1257 abnormalities of far-field auditory brainstem responses. *Electroencephalogr Clin Neurophysiol*
1258 41: 595-608, 1976.

1259 **Suzuki T, Hirai Y, and Horiuchi K.** Auditory brain stem responses to pure tone stimuli. *Scand*
1260 *Audiol* 6: 51-56, 1977.

1261 **Tateuchi T, Itoh K, and Nakada T.** Neural mechanisms underlying the orienting response to
1262 subject's own name: an event-related potential study. *Psychophysiology* 49: 786-791, 2012.

1263 **Thorpe SG, Nunez PL, and Srinivasan R.** Identification of wave-like spatial structure in the
1264 SSVEP: comparison of simultaneous EEG and MEG. *Stat Med* 26: 3911-3926, 2007.

1265 **Tiitinen H, Sinkkonen J, Reinikainen K, Alho K, Lavikainen J, and Naatanen R.** Selective
1266 attention enhances the auditory 40-Hz transient response in humans. *Nature* 364: 59-60, 1993.

1267 **Van Der Tweel LH, and Lunel HF.** Human Visual Responses to Sinusoidally Modulated Light.
1268 *Electroencephalogr Clin Neurophysiol* 18: 587-598, 1965.

1269 **Vanni S, Warnking J, Dojat M, Delon-Martin C, Bullier J, and Segebarth C.** Sequence of
1270 pattern onset responses in the human visual areas: an fMRI constrained VEP source analysis.
1271 *Neuroimage* 21: 801-817, 2004.

1272 **Vaughan HG, Jr., and Ritter W.** The sources of auditory evoked responses recorded from the
1273 human scalp. *Electroencephalogr Clin Neurophysiol* 28: 360-367, 1970.

1274 **Vialatte FB, Maurice M, Dauwels J, and Cichocki A.** Steady-state visually evoked potentials:
1275 focus on essential paradigms and future perspectives. *Prog Neurobiol* 90: 418-438, 2010.

1276 **Weber BA, and Folsom RC.** Brainstem wave V latencies to tone pip stimuli. *J Am Audiol Soc*
1277 2: 182-184, 1977.

1278 **Woldorff M, Hansen JC, and Hillyard SA.** Evidence for effects of selective attention in the
1279 mid-latency range of the human auditory event-related potential. *Electroencephalogr Clin*
1280 *Neurophysiol Suppl* 40: 146-154, 1987.

1281 **Woldorff MG, and Hillyard SA.** Modulation of early auditory processing during selective
1282 listening to rapidly presented tones. *Electroencephalogr Clin Neurophysiol* 79: 170-191, 1991.

1283 **Woods DL, Alain C, Covarrubias D, and Zaidel O.** Frequency-related differences in the speed
1284 of human auditory processing. *Hear Res* 66: 46-52, 1993.

1285 **Yoshiura T, Ueno S, Iramina K, and Masuda K.** Human middle latency auditory evoked
1286 magnetic fields. *Brain Topogr* 8: 291-296, 1996.

1287 **Yoshiura T, Ueno S, Iramina K, and Masuda K.** Source localization of middle latency auditory
1288 evoked magnetic fields. *Brain Res* 703: 139-144, 1995.

1289 **Zhu L, Bharadwaj H, Xia J, and Shinn-Cunningham B.** A comparison of spectral magnitude
1290 and phase-locking value analyses of the frequency-following response to complex tones. *J*
1291 *Acoust Soc Am* 134: 384-395, 2013.

1292

1293

1295 **Table 1. ERP Results.** Summary of single-subject results and group peak measurements
 1296 (amplitude and latency) for each component. The “number of subjects” column indicates the
 1297 number of subjects (out of 25) that showed a significant response for each component (using a
 1298 p-threshold of 0.001). For the sustained components, the reported amplitude reflects an
 1299 average across time (~225-425 ms for LLR Sustained Negativity; ~420-500 ms for VEP Late
 1300 Negativity), instead of the peak amplitude.

ERP Response	Component	Number of Subjects	Peak Amplitude: Mean (μV)	Peak Amplitude: Standard Error (μV)	Peak Latency: Mean (ms)	Peak Latency: Standard Error (ms)
ABR (Cz)	n ₀	24	-0.25	0.015	3.45	0.086
	Wave V	25	+0.40	0.024	6.51	0.076
	N ₀	25	-0.29	0.014	8.95	0.098
	P ₀	16	+0.12	0.015	13.0	0.105
MLR (Fz)	Na	22	-0.44	0.047	17.8	0.29
	Pa	17	+0.23	0.046	25.0	0.31
	Nb	17	-0.23	0.052	33.4	0.43
	Pb	20	+0.31	0.042	44.1	0.32
LLR (Fz)	P1	25	+1.77	0.11	80	2.3
	N1	21	-0.66	0.11	173	2.6
	Sustained Negativity	23	-0.64 (average)	0.08 (SE of average)	323	11.4
VEP (Oz)	P1	22	+3.65	0.39	106	2.3
	N1	17	-2.31	0.47	177	3.0
	P2	20	+2.54	0.45	250	2.7
	Late Negativity	20	-1.62 (average)	0.31 (SE of average)	468	4.7

1301 **Table 2. Steady-State Results.** Summary of single-subject results, as well as the group
 1302 magnitudes and signal-to-noise ratios (SNRs) at each frequency of interest of the ASSR and
 1303 SSVEP. The “number of subjects” column indicates the number of subjects (out of 25) that
 1304 showed a significant response for each component (using Bonferroni-corrected p-thresholds).
 1305 These results were derived from the magnitude spectra and noise floor estimates that were
 1306 averaged in frequency space across epochs and draws, within the bootstrapping algorithm.

Steady-State Response	Frequency (Hz)	Number of Subjects	Raw Magnitude: Mean (dB, arbitrary units)	Raw Magnitude: Standard Error (dB, arbitrary units)	SNR: Mean (dB)	SNR: Standard Error (dB)
ASSR (Fz)	41	25	-18.8	0.90	16.4	0.82
	82	24	-25.6	1.18	12.7	1.22
	123	25	-27.6	0.67	13.2	0.63
	164	25	-28.5	0.55	14.7	0.62
SSVEP (Oz)	7.5	21	-11.5	0.65	3.8	0.50
	12	24	-13.5	0.64	3.4	0.43
	15	22	-10.9	1.08	7.3	0.90
	24	19	-17.4	0.91	4.1	0.67

1307

1308

1309

1310

1311

1312

Figure Captions

1313

1314 **Figure 1. Stimuli and Experimental Design.** **A)** Examples of the Black/White (left) and
1315 Red/Green (right) stimuli are displayed. **B)** A spectrogram of the Cheech is shown on the left
1316 for one of the sentences. On the right, a zoomed-in view of a chirp train is illustrated, to
1317 demonstrate that the second chirp in each train was omitted for recording a clear auditory MLR.
1318 **C)** An overview of the stimulus presentation is depicted.

1319 **Figure 2. ABR Results.** **A)** Single-subject ABRs in channel Cz are shown, thresholded at $p <$
1320 0.001, with non-significant data samples set to an amplitude of 0 μV . **B)** Group-average ABRs
1321 derived from the bootstrapping procedure are shown. The top panel shows the group-average
1322 time waveform, while the group-average scalp topographies of the significant deflections are
1323 displayed below. In this figure and in Figures 3, 4, and 5, the gray shaded box in the group time
1324 waveform plot depicts the group average (plus standard error of the mean) range of amplitudes
1325 that were not significant, using a p -threshold of 0.001.

1326 **Figure 3. MLR Results.** **A)** Single-subject MLRs in channel Fz are shown, thresholded at $p <$
1327 0.001, with non-significant data samples set to an amplitude of 0 μV . **B)** The group-average
1328 MLR time waveform is shown, along with the scalp topographies of the significant MLR
1329 components.

1330 **Figure 4. LLR Results.** **A)** Single-subject LLRs in channel Fz are shown, thresholded at $p <$
1331 0.001, with non-significant data samples set to an amplitude of 0 μV . **B)** The group-average
1332 LLR time waveform is displayed, along with the scalp topographies of the auditory P1 and
1333 N1/sustained negativity.

1334 **Figure 5. VEP Results.** **A)** Single-subject VEPs in channel Oz are displayed, which have been
1335 thresholded at $p <$ 0.001, with non-significant data samples set to an amplitude of 0 μV . **B)** The

1336 group-average VEP time waveform is shown, along with the scalp topographies of the
1337 significant VEP components

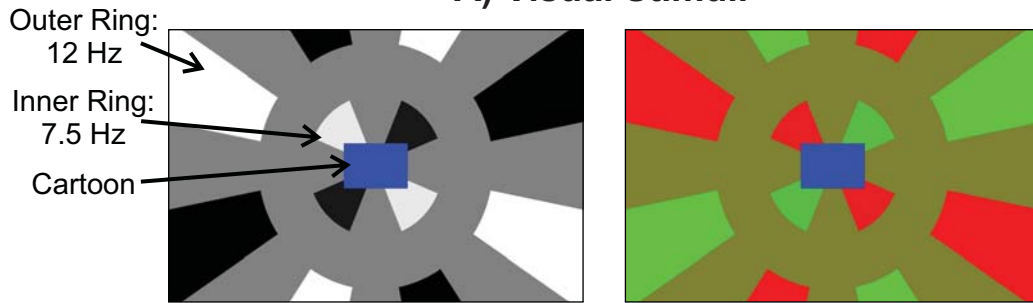
1338 **Figure 6. ASSR Results. A)** Single-subject data, indicating signal-to-noise ratio of the 41 Hz
1339 ASSR and the first three harmonics (82, 123, and 164 Hz), are displayed, for channel Fz. Non-
1340 significant responses were set to 0 dB; note that only one participant had a non-significant
1341 ASSR: Subject 16 at 82 Hz. **B)** Group-average raw ASSR magnitude and the signal-to-noise
1342 ratio, along with the noise floor estimate, are depicted; these responses were created by
1343 averaging data in the frequency domain. Additionally, the raw magnitude computed by
1344 averaging data in the time domain before converting to the frequency domain, is plotted. Below
1345 are the group-average scalp topographies of the raw ASSR magnitude (averaged in the
1346 frequency domain) at the four frequencies of interest. Abbreviations: SNR, signal-to-noise ratio;
1347 n.s., not significant.

1348 **Figure 7. SSVEP Results. A)** Single-subject responses, indicating signal-to-noise ratio at 7.5
1349 Hz (inner ring), 12 Hz (outer ring), 15 Hz (inner ring harmonic), and 24 Hz (outer ring harmonic)
1350 are displayed, for channel Oz. Non-significant SSVEP responses were set to 0 dB. **B)** Group-
1351 average raw SSVEP magnitude and the signal-to-noise ratio, along with the noise floor
1352 estimate, are depicted; these responses were created by averaging data in the frequency
1353 domain. Additionally, the raw magnitude computed by averaging data in the time domain before
1354 converting to the frequency domain, is plotted. Below are the group-average scalp
1355 topographies of the raw SSVEP magnitude (averaged in the frequency domain) at the four
1356 frequencies of interest. Abbreviations: SNR, signal-to-noise ratio; n.s., not significant.

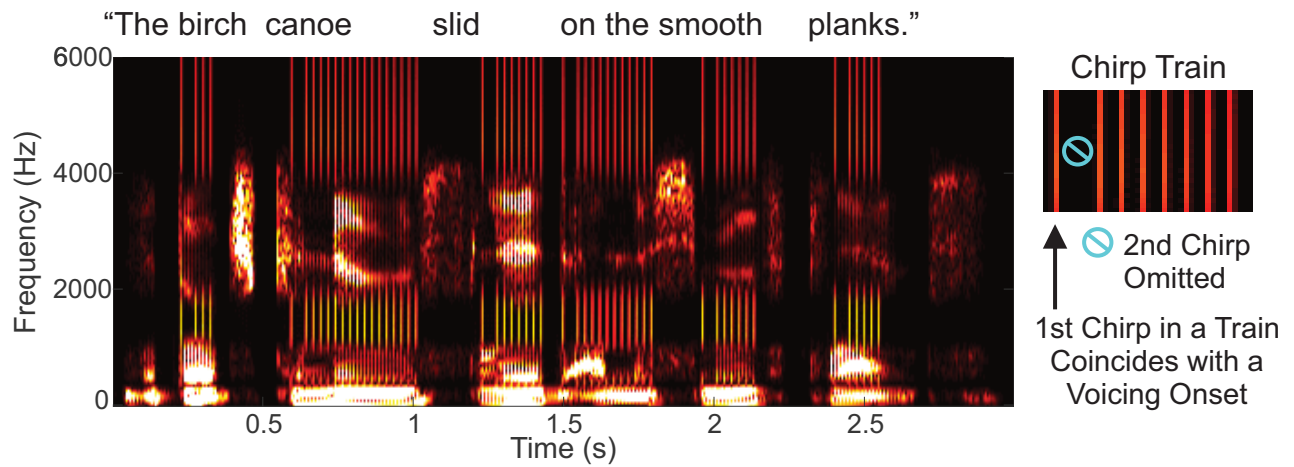
1357 **Figure 8. Z-Scored Single-Subject Data.** Aggregate z-scores for each EEG response are
1358 plotted for each subject.

1359

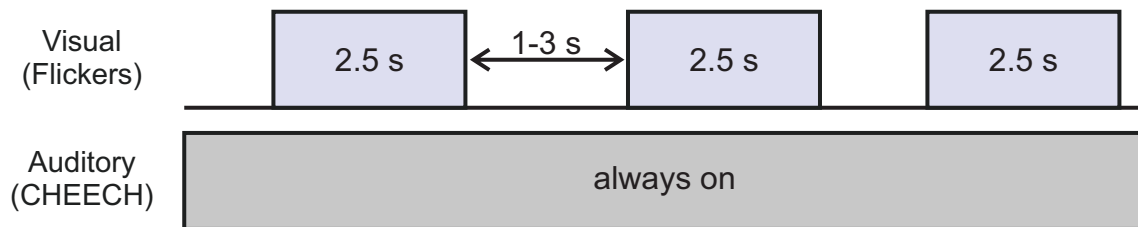
A) Visual Stimuli



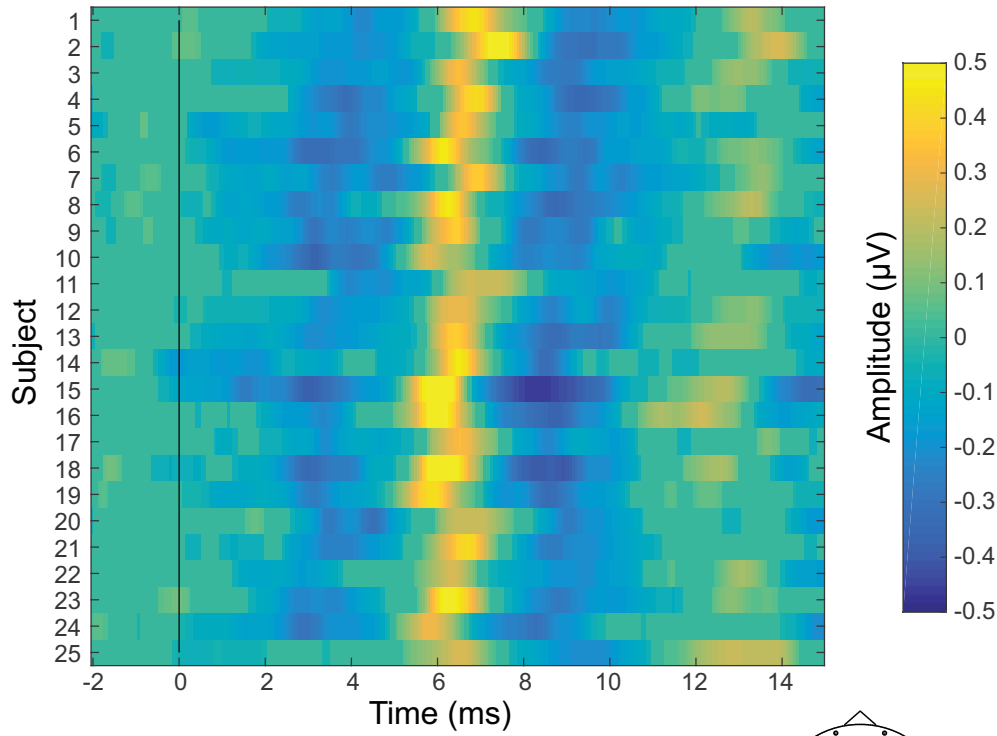
B) Auditory Stimuli: CHEECH (CHirp-spEECH)



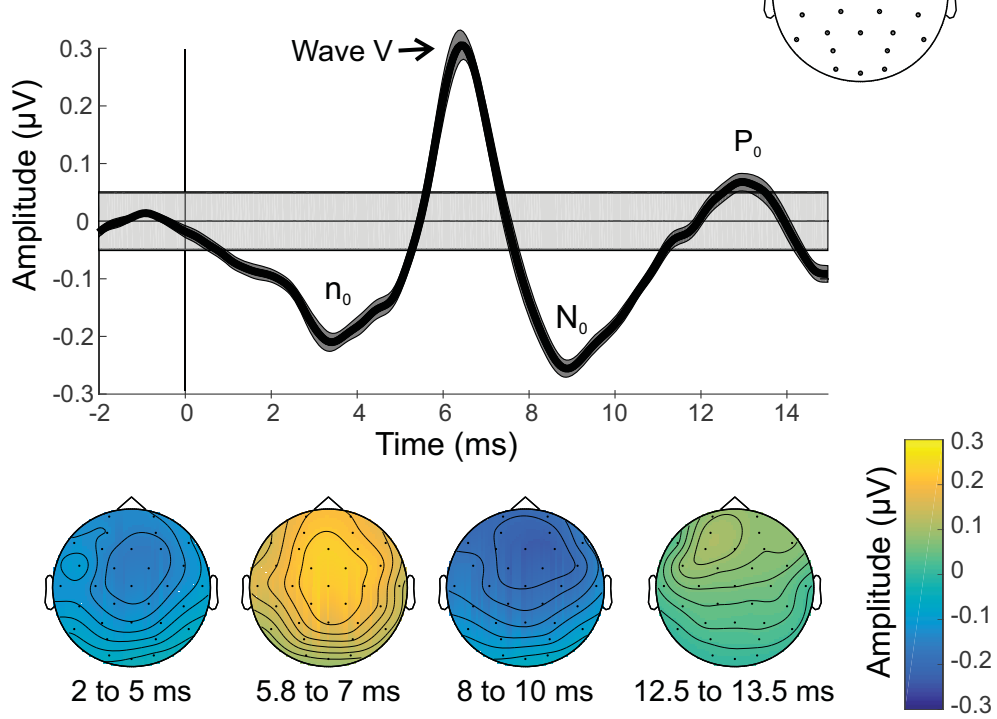
C) Overview of Stimulus Presentation



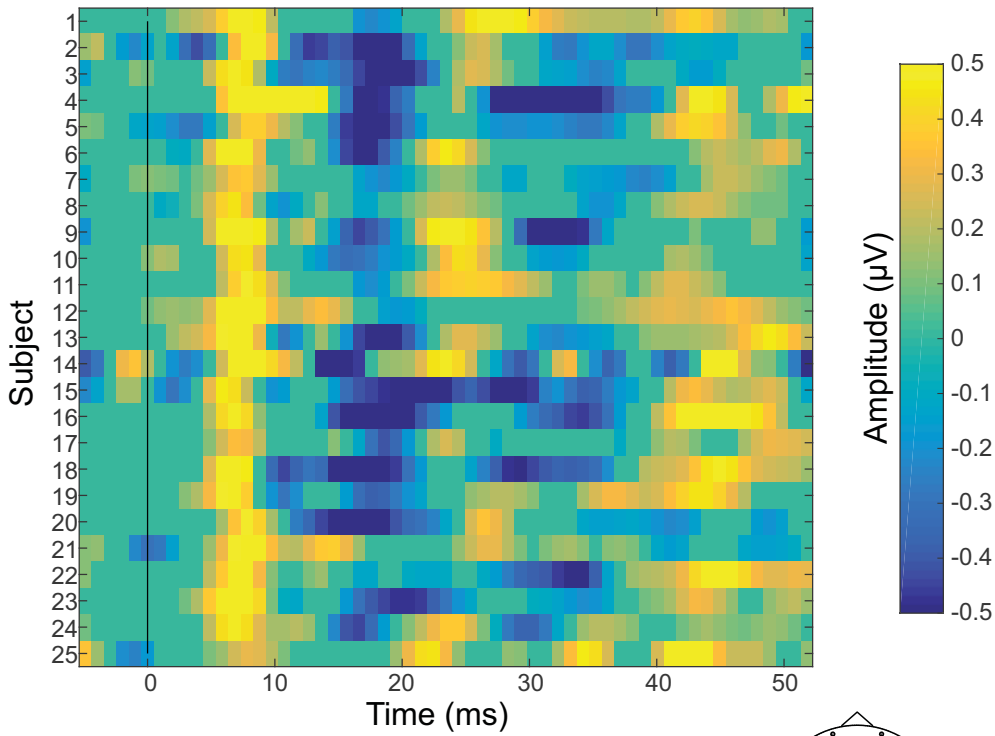
A) Single Subject ABR Results



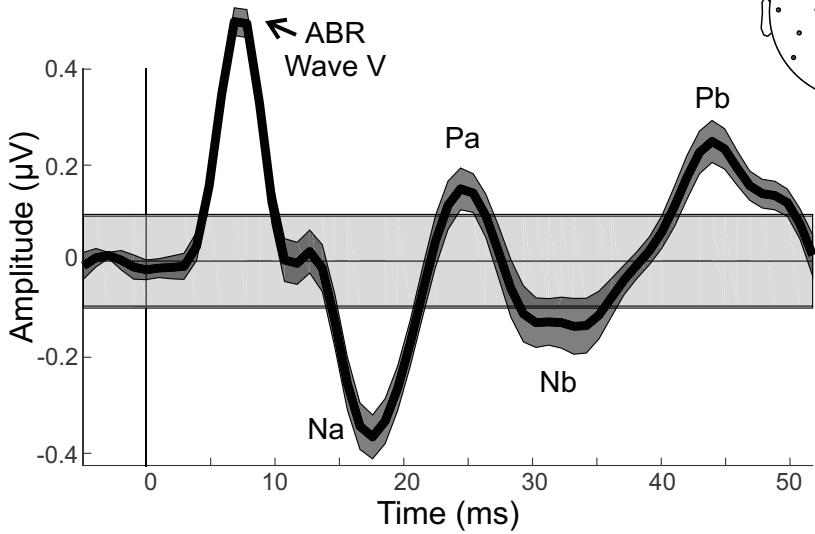
B) Group Average ABR



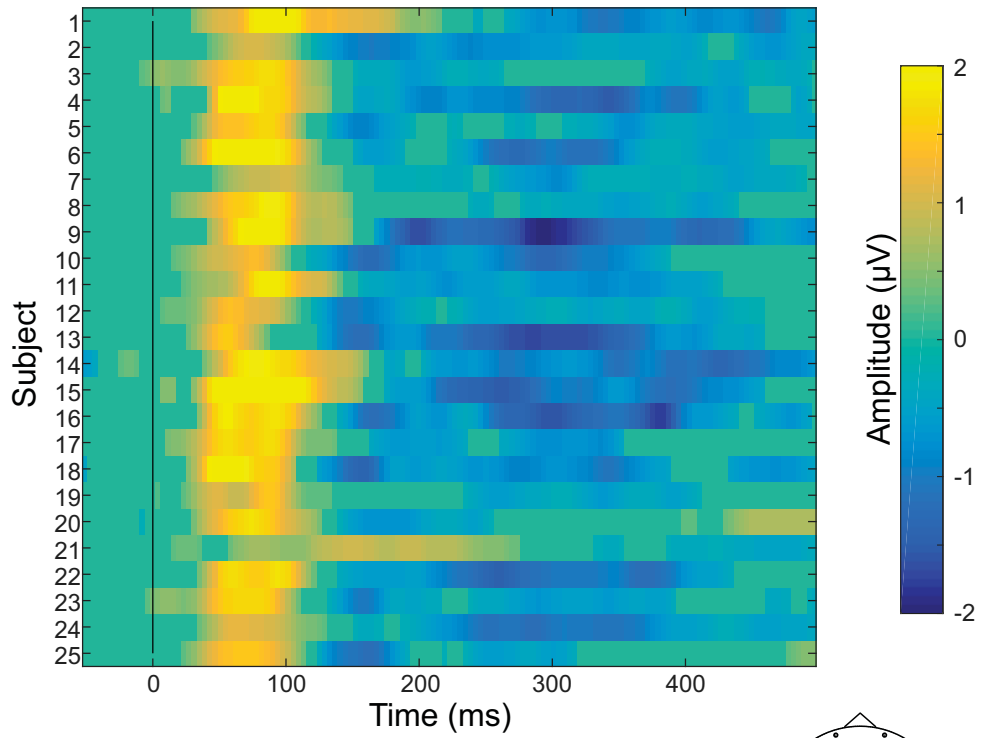
A) Single Subject MLR Results



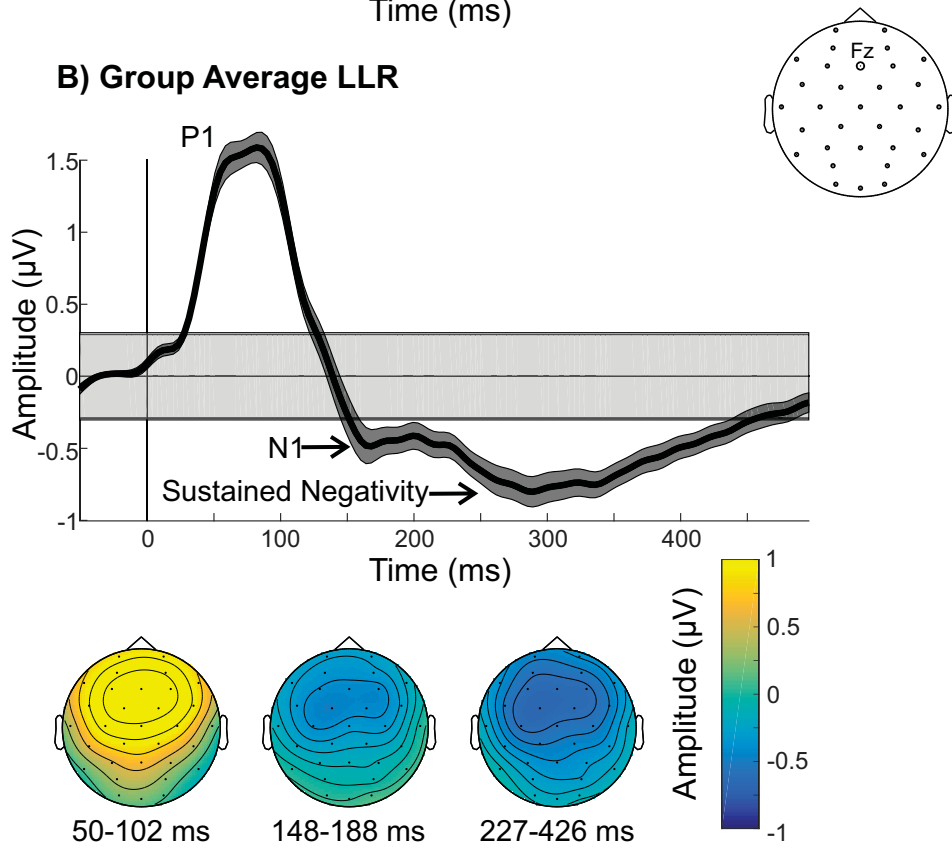
B) Group Average MLR



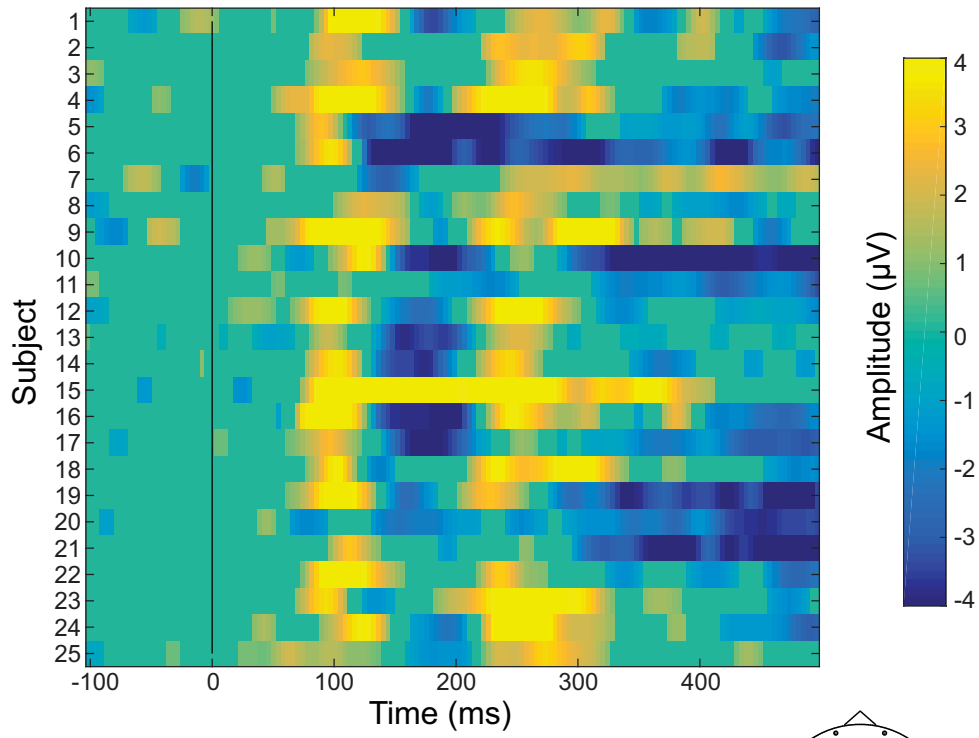
A) Single Subject LLR Results



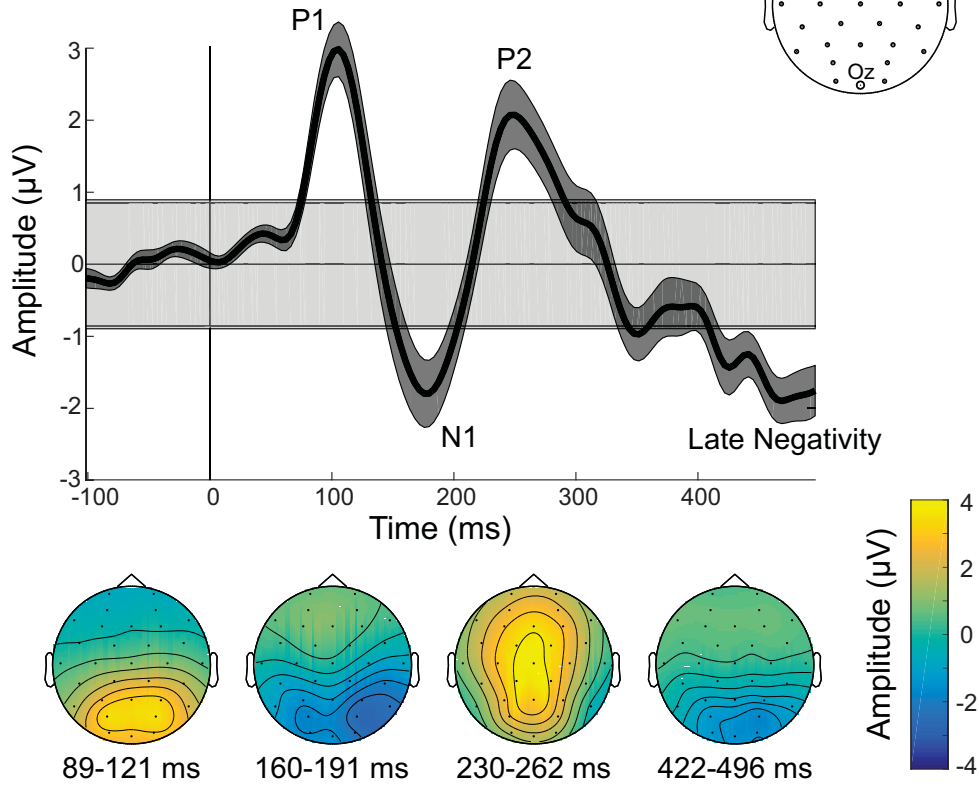
B) Group Average LLR



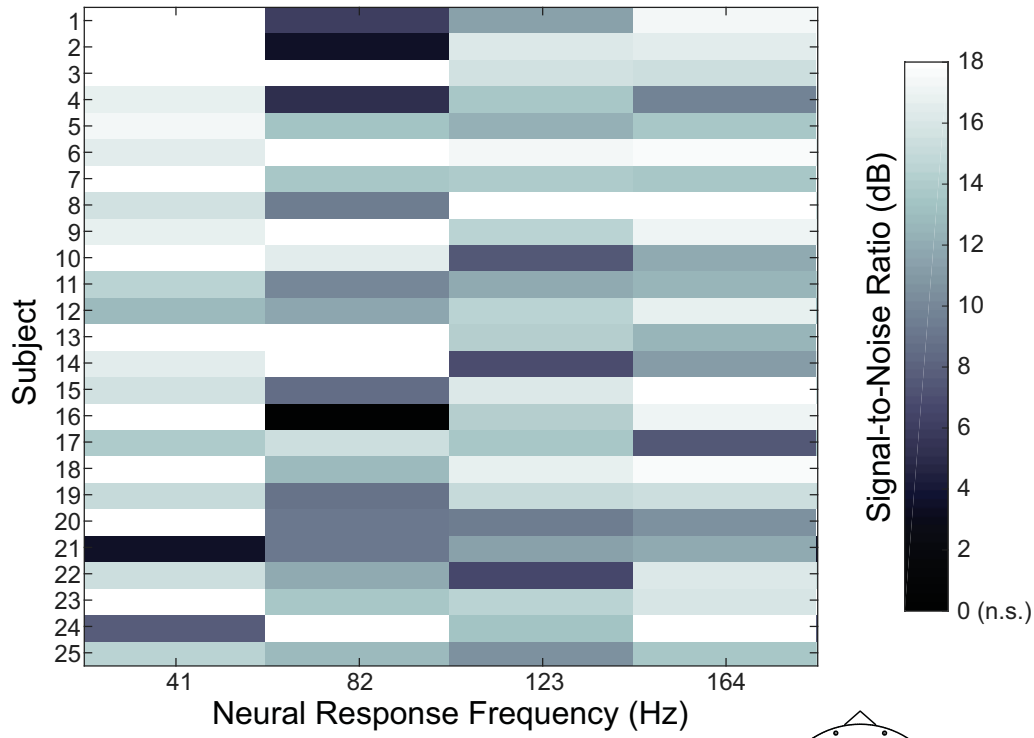
A) Single Subject VEP Results



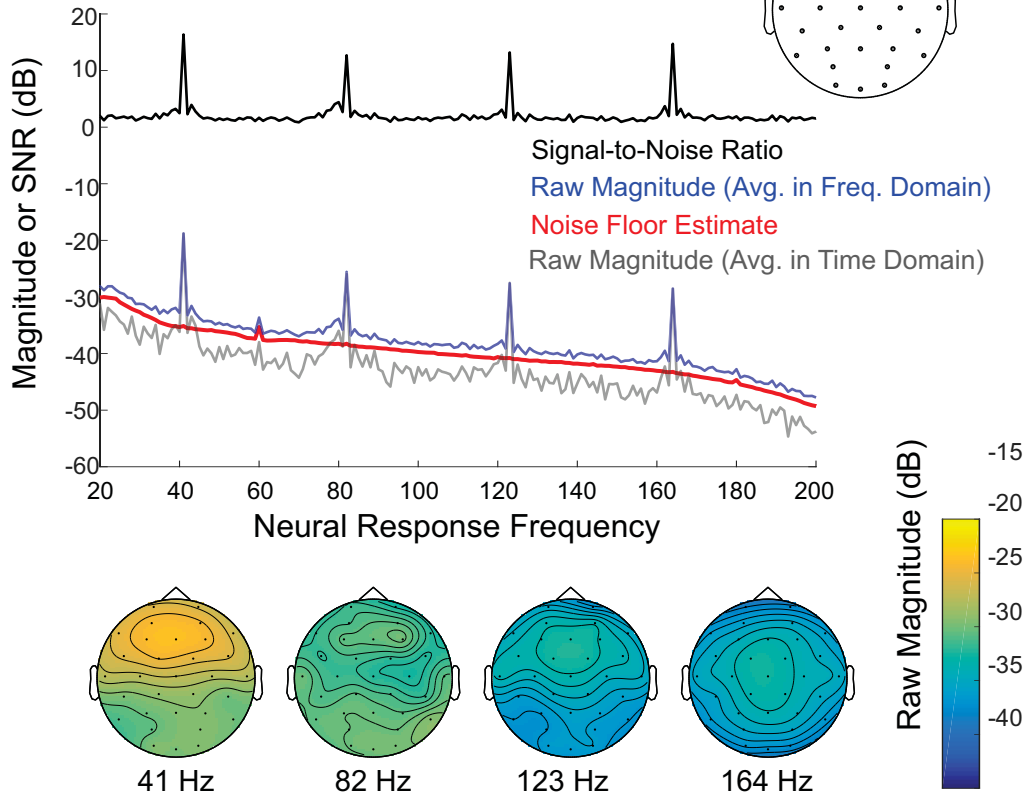
B) Group Average VEP



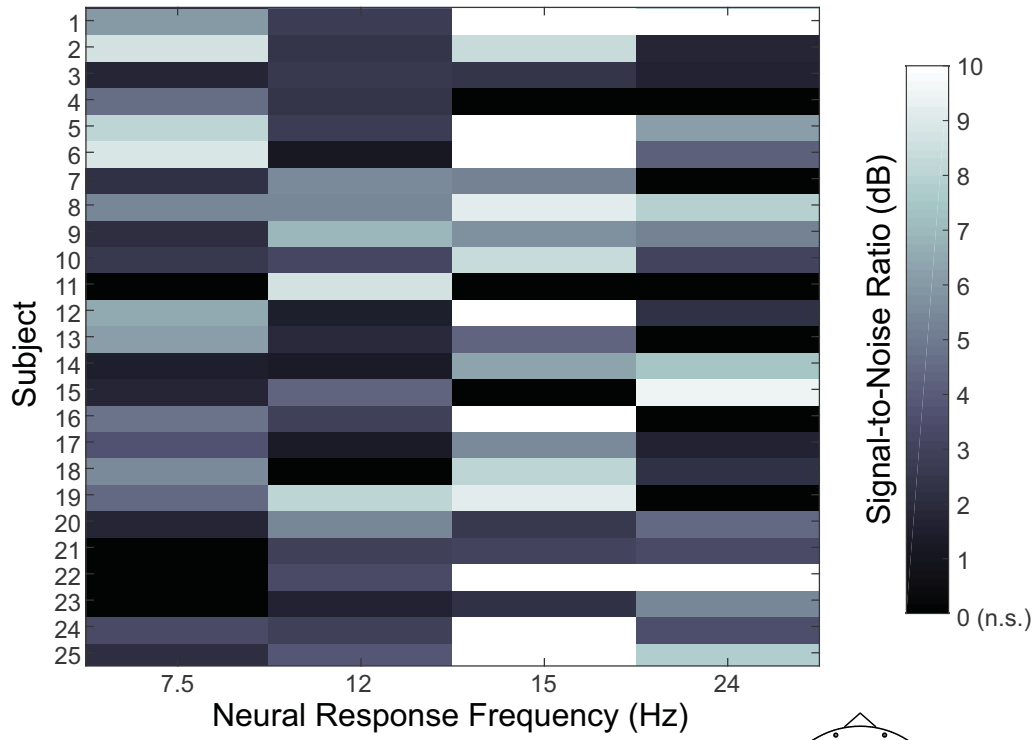
A) Single Subject ASSR Results



B) Group Average ASSR



A) Single Subject SSVEP Results



B) Group Average SSVEP

